HASTECS

Hybrid Aircraft Academic reSearch on Thermal & Electrical Components and Systems

Clean Sky

Mars 2019

Malik Tognan, Christophe Turpin (Laplace)
Patrice Simon (Cirimat)

Preliminary delivery Battery & Fuel Cell metamodels; "HASTECS M6.1" Technical report

cnrs Laplace INP ENSEEIHT Université de Toulouse AIRBUS

SUMMARY

ABBREVIATIONS / SYMBOLS

BMS: Battery Management System

BoP: Balance of Plants

DOD: Depth Of Discharge (%)

DOE: Department of Energy

FC: Fuel Cell

HT / LT: High Temperature (140 – 180 °C) / Low Temperature (60 – 80 °C)

LH_2: Liquid H_2

LHV: Lower Heating Value of hydrogen (33.3 kWh/kg)

LiS: Lithium Sulfur

LTO: Lithium Titanate Oxide (anode material)

MEA: Membrane Electrode Assembly

MLI: Multi-Layer Insulation

NMC: Nickel Manganese Cobalt (cathode material)

PEM FC: Proton Exchange Membrane Fuel Cell

SOC: State Of Charge (%)

SOFC: Solid Oxide Fuel Cell

SSB: Solid State Battery (also refered as All solid state)

TNO: Titanium Niobium Oxide (anode material)

1. INTRODUCTION

The work presented in this document is a part of the Hastecs project (Hybrid aircraft Academic reSearch on Thermal & Electrical Components and Systems) dedicated to the development of models and tools that can support the demonstration of radical aircraft configurations. More specifically, the case of a hybrid-electric aircraft with a serial-hybrid configuration (all the energy conversion chain is electrified) is treated here. Inside this project divided in six Work Packages (WPs), the Work Package n°6 is dedicated to the global system integration (Matthieu Pettes-Duller pHD work) and to the auxiliary source which is going to hybridize the main power source (the gas turbines). The report developed here, conclusion of a one year post-doctorate work, is treating the case of this auxiliary source consisting of a Battery and/or a Fuel Cell (FC) with a H_2 storage system.

Two objectives are followed in this study:

- A state of the art of the current and future performances of battery and fuel cell systems in aeronautic and more generally in embedded applications (especially automotive ones).
- The development of modeling tools to identify the behavior of the hybrid source and to estimate its mass.

Obviously the two objectives are intimately linked, as the development of modeling tools relies on empirical data coming from the state of the art. In this report, a particular focus is laid on the state of the art while the modeling developments are summarized in a more synthetical way. A selection of Li-ion battery technologies, from high power type to very high energy type, as well as a selection of FC technologies is firstly considered for the state of the art step in order to assess typical performances values in terms of specific energies and powers. H_2 storages media are as well considered regarding their gravimetric efficiencies performances. Various articles and datasheet are scanned in order to assess average values and progression margin for the next decades. A specific attention is given to the contextualization of all the power and energy specific values regarding parameters such as charge and discharge speed capabilities (C_{rate}) for the different battery technologies, or FC system structure regarding the different auxiliary components for the FC technologies.

A first-level modeling based on simplified equations is then proposed to assess different sizing and system mass estimations of the auxiliary source considering two emblematic power missions corresponding to a light-hybridization scenario. Thereafter, second-level modeling developments are introduced in order to refine the previous results and to provide more insights into the auxiliary source behavior regarding parameters such as efficiency, State of Charge, auxiliary components parasitic consumptions, etc. Conclusions are finally given considering the state of the art values and the masses assessment for the different technologies.

2. STATE OF THE ART OF THE POWER AND ENERGY DENSITIES OF BATTERY / FUEL CELL SYSTEMS FOR EMBEDDED APPLICATIONS TODAY AND TOMORROW

Two different kinds of assessments have to be done for both battery and FC systems: whereas a battery system exhibits an intrinsic coupling between its energy and power capabilities, a FC system is separated between its power conversion stage and its energy storage (H_2 storage). Consequently, separate assessments of FC stacks power performances on one hand and H_2 storage capabilities on the other hand need to be addressed.

The following paragraphs will thus detail separately the states of the art of current battery performances on one hand, and of FC stacks and systems together with H_2 storage systems capabilities on the other hand.

2.1. Preliminary definitions

In order to quantify the battery/FC performances, a few parameters are going to be scanned:

- The gravimetric and volumetric energy densities (specific energy) – $e_m(Wh/kg)$ and $e_v(Wh/L)$ – represent for a given energy source or energy container its intrinsic energy content with respect respectively to its mass and volume.
- The gravimetric and volumetric power densities (specific power) – $p_m(W/kg)$ and $p_v(W/L)$ – represent, in a complementary manner, for a given power source its intrinsic ability to deliver a certain power with respect to its mass and volume.
- The C_{rate} expresses the speed of charge/discharge of a battery: a C_{rate} is independent of the battery capacity (size) and current and is homogeneous to a frequency (h^{-1}). For instance, a battery discharge at a C_{rate} of 1 C means that the battery will be discharged in one hour, at 0.2 C in 5 hours, at 2 C in 30 minutes… The C_{rate} capabilities of a battery are thus closely linked to its specific power performances: the ability to charge/discharge at a certain C_{rate} a certain amount of energy is equivalent to a power capability.
- For the H_2 storages medias: the gravimetric index – $\eta_m(-)$ often expressed as "wt. %" – represent the amount of H_2 kg that can be stored with respect to the total mass (including the H_2 contained inside) of the storage system:

$$\eta_m = \frac{kg_{H_2}}{kg_{storage\ system}} \quad (1)$$

2.2. State of the art of battery specific power and energy performances in mobile applications (automotive and aeronautical)

Battery performances do not only consist in its specific energy and/or power but also rely on cyclability aspects (how the battery capacity / internal resistance are going to decline with the accumulation of working cycles). Even if these aspects are of first importance they may not be treated as well as those mentioned earlier, mainly because cyclability data is often less

available or incomplete. Also, several battery technologies – such as Lead-acid, Ni-Zn, flow batteries… – will not be considered in the global overview considering their too small energy densities.

2.2.1. Overview of the general battery performances statements today and tomorrow in scientific articles and reviews

In a first attempt to evaluate the battery performance assessments made in the literature, it can be relevant to have a look on how these assessments are actually made in articles exploring themes close to the main study thematic (hybrid-electric propulsion, electric flight…). More specifically, the idea is to aggregate, between the articles investigating on a future electrical propulsion or on the integration of battery systems in aircrafts, the values of the batteries specific gravimetric and volumetric energy/power densities taken as references, as well as the technologies mentioned.

2.2.1.1. Assumptions made in articles investigating on the electric flight and/or studying hybrid-electric aircraft concepts

In [KUH-12], the authors investigate the fundamental prerequisites for electric flying and the potential of hybrid power systems for air transport. A review of battery negative and positive electrode material is made in order to highlight the different combinations possible and the most energetic ones theoretically achievable (Figure 1).

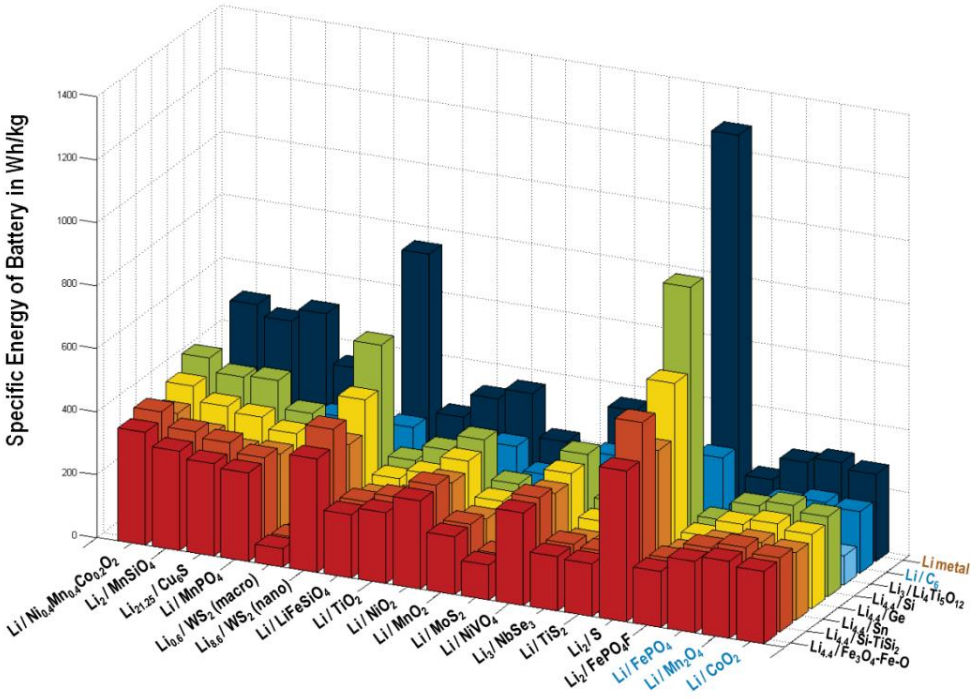

Figure 1 - Combinatory analysis of different materials for negative (right axis) and positive (left axis) electrodes with their corresponding theoretical specific energies (y-axis); picture from [KUH-12]

The authors highlight for instance that while graphite is still today the most used material for the negative electrode, materials such as Silicon are the most promising to increase the

electrode capacity. Even if the Li metal negative electrode is supposed to bring the best specific energies on the paper (Figure 1), the authors underline that for safety reasons (dendrites build-up risks) this option is not used in commercial cells. For the positive electrode, materials such as Sulfur and Nickel Manganese Cobalt (NMC) metal oxides are mentioned as the most promising ones to increase the cell specific energy. The authors assert that with a combination of these materials, a maximum of about 350 Wh/kg can be easily achieved at the cell scale (with a limit at 1 kWh/kg). For the high power capabilities, Lithium Iron Phosphate (LFP) batteries are said to present very impressive specific powers (up to 90 kW/kg at 200 C) by the same authors. Nevertheless, Lithium Titanate Oxide technologies show today better power performance and safety (only small SEI), and more potential gain in performance in the future (LFP is close to its maximal performances).

Several studies ([HEP-12] and [STU-12]), also focused on the potential of electric flight, mention technologies such as Lithium Sulfur and Lithium-Air as the most promising for the future, with specific energies rising up to 1700 Wh/kg in 2025-2030 for the latest (Lithium-Air) at the cell level. This value is used as well in [POR-15], where concepts of hybrid electric flights are also investigated. More recently, publications anticipating the future performances of battery systems respectively in 2030 and 2035, such as [HOE-18] or [MUE-18], mention as well the Lithium-Air and the Lithium-Sulfur technologies. The development of the Lithium-Air seems however quite challenging today because of superoxide productions.

The high expectations are put up to 1 kWh/kg (with 1 kW/kg for the power capabilities) in [HOE-18] for Lithium-Air and 0.65 kWh/kg / 1 kW/kg for Lithium-Sulfur, while [MUE-18] focus only on Lithium-Sulfur with values such as 0.5 kWh/kg (0.6 kWh/L) / 1 kW/kg (all these values are considered at the system scale, including the packaging and cooling mass).

Unlike the previous studies, [KUH-12] seems more precautious with the Lithium-Air battery, pointing out practical limits such as a 600Wh/kg barrier for the specific energy and also a very poor specific power (in the range of mW/kg). **These poor power capabilities of the Lithium-Air battery are, for the authors, a clear showstopper for aviation applications**.

After this first overview of the battery performances assumptions taken by prospective studies on electrified aircraft, a closer look will be given on papers exclusively focused on the different available battery technologies and their current and expected performances.

2.2.1.2. Reviews focused on the battery performances evolution and trends

In their review, Le Cras and Bloch ([LEC-15]) give an overall picture of the development of Lithium-ion battery technologies in the last decades and show in one of their tables some orders of magnitudes for embedded batteries in the automotive context (Figure 2).

This first list gives us some insights about the current performances of embedded Li-ion battery systems: from 89 Wh/kg for a “power type” battery such as Lithium Titanate Oxide (LTO) to 233 Wh/kg for High Energy type like Nickel Cobalt Aluminum (NCA). The authors

underline furthermore current trends of investigation to increase the cell specific energy: the use of Li-metal for the negative electrode, as well as Sulfur or Air for the positive one.

Tableau 4 – Différents types de cellules Li-ion pour VE ou VEH commercialisés en 2015										
Fabricant	Chimie (anode/cathode)	Capacité (Ah)	Type	Tension (V)	Masse (kg)	Volume (L)	Densité d'énergie (Wh/L)	(Wh/Kg)	Utilisé dans : Fabricant	Modèle
AESC	G/LMO-NCA	33	Polymère	3,75	0,80	0,40	309	155	Nissan	Leaf
LG Chem	G/NMC-LMO	36	Polymère	3,75	0,86	0,49	275	157	Renault	Zoe
Li-Tec	G/NMC	52	Polymère	3,65	1,25	0,60	316	152	Daimer	Smart
Li Energy Japan	G/LMO-NMC	50	Prismatique	3,7	1,70	0,85	218	109	Mitsubishi	i-MiEV
Samsung	G/NMC-LMO	64	Prismatique	3,7	1,80	0,97	243	132	Fiat	500
Lishen Tianjin	G/LFP	16	Prismatique	3,25	0,45	0,23	226	116	Coda	EV
Toshiba	LTO/NMC	20	Prismatique	2,3	0,52	0,23	200	89	Honda	Fit
Panasonic	G/NCA	3,1	Cylindrique	3,6	0,05	0,02	630	233	Tesla	Modèle S

Figure 2 - List of Li-ion cells chemistries used in electrical or hybrid-electrical vehicle in 2015 ([LEC-15])

In [PER-18], among the description of technologies such as Lead-acid, Ni-Mh, Ni-Zn, several orders of magnitude are given for Li-ion batteries (up to 250 Wh/kg at the cell scale) as well as for Lithium Sulfur (300 Wh/kg at the cell scale with reachable targets between 400 – 600 Wh/kg). The author highlights the poor cyclability of the Lithium Sulfur (not more than 300 cycles to date). The all solid state battery, composed of a solid electrolyte, Li-metal on the negative electrode instead of graphite, and the same chemistry as the usual Li-ion ones – NMC, NCA… – for the positive electrode, is also mentioned as an upcoming technology, even if the main limitation seems to be the working temperature of the electrolyte (usually a high temperature because of the polymer electrolyte). For the all solid state battery, values such as 400 Wh/kg can be expected according to the author.

As reported in [MIS-18], current performances for high energy Li-ion battery such as NMC are today around 250 Wh/kg at the cell level and 150 Wh/kg at the system scale (Tesla is said to have reached the best specific energy – 170 Wh/kg – at the pack level). Changing the anode material for Li-metal or the use of silicon-base composite (few at% of Si) together with a high Ni NMC cathode (Ni-rich) should, according to the author, bring specific energies up to 350 Wh/kg at the cell scale in the next decade. Unlike [HOE-18] or [MUE-18], **the author affirm that the value of 1 kWh/kg is not seemingly possible even in the next 20, 30 years**.

In [FUS-15], a large overview of the different battery technologies for future aircraft propulsion is given as well as a concrete state of the art and projected numbers of specific energies, specific powers, energy density and cyclability. The author underlines particularly the current limits of high energy Li-ion batteries (around 220-280 Wh/kg_{cell}), as well as some orders of magnitude for high power Li-ion batteries (from 2 to 7 kW/kg_{cell} for technologies such as LFP and/or using Lithium Titanate Oxide – LTO anodes). The global review highlights some global tendencies such as the good cyclability of high power batteries compared to the high energy ones.

The poor cyclability of LiS is also mentioned as well as its low volumetric energy and specific power. Interestingly, the author presents some roadmaps for the high energy / high

power batteries from today to 2020-2025: the following table details briefly some information contained in these roadmaps (Table 1).

		Li-ion High Energy	Li-ion High Power	Li-S
Today	Cell scale	< **250 Wh/kg** (300 Wh/kg under development)	50 Wh/kg ; **2 kW/kg** ; >10000 cycles	~ **300 Wh/kg** (C/10) ; ~ 300-400 Wh/L ; 10-50 cycles
	System scale	~ **150 Wh/kg** ; 230 Wh/L ; 750 cycles	–	–
Tomorrow (2020 or 2025)	Cell scale	**500 Wh/kg** ; 1500 Wh/L ; (2025)	70 Wh/kg ; **6 kW/kg** ; 10000 cycles (2020)	**600 Wh/kg** ; 700 Wh/L ; 2000 cycles (2025)
	System scale	**290 Wh/kg** ; (< 270 Wh/kg) 375 Wh/L ; 200-500 cycles (2020)	–	**400 Wh/kg** ; (< 330 W/kg) 300-500 cycles (2025)

Table 1 - High Energy / High Power Li-ion technologies roadmap synthesis from [FUS-15]

As the table presents a compilation of some values seen in three or four roadmaps, all the data (number of cycles, energy volumetric density…) are not systematically available for each kind of Li-ion batteries. The perspectives at the cell and system scale for the "High Energy" column are quite high (500 Wh/kg_{cell} and 290 Wh/kg_{system} for 2025 and 2020 respectively) and correspond to the projections for the solid-state Li-metal batteries (not mature yet). For non-solid-state technologies, there is today a consensus about the values: 350 Wh/kg_{cell} with same cyclability (>1,000) and so on seems to be the maximal reachable. With lower cyclability (<1,000), 400 Wh/kg_{cell} can be reachable with Si anode. For the "High Power" column, the data refer to LTO technologies. The Lithium Sulfur (LiS) column is also added to the table as it represents the Li-ion technology with the highest predicted specific energy together with Li-Air. The projections for the Li-Air battery (not mentioned in Table 1) are lower than in [HEP-12] and [STU-12], with a value such as 500 Wh/kg_{system} expectable around 2035.

To sum up, similar orders of magnitude are given in all these reviews ([FUS-15], [MIS-18], [PER-18], [LEC-15]) for the current performances of High-Energy Li-ion batteries (250 Wh/kg_{cell} and 150 Wh/kg_{system}) and other technologies such as Li-S (300 Wh/kg_{cell} achievable today and 400-600 Wh/kg_{cell} in the next decade).

Even if a global consensus is coming from the values seen in all the reviews mentioned (except for the long term projections of Li-Air), it is sometimes hard to contextualize them: what is the exact behavior of each Li-ion technologies when changing the C_{rate} in terms of specific energy and durability? What are the specific power values exactly referring to (max peak power or continuous discharge/charge power)?

Some of these interrogations remain a bit cloudy and would require more precise insight through discharge/charge characteristics of specific cells for example.

Several technologies for each type of Li-ion batteries have also been mentioned in a recurrent manner:

- Very high energy: Li-S, Lithium-Air, Li-metal anode with high energy cathode
- High energy: NMC, NCA, Li-rich cathodes
- High power: LTO anode, LFP

In order to refine the bibliographic review and to have a concrete look on each type of Li-ion batteries, three typical technologies are selected: Li-S for the very high energy type, NMC for the high energy type and LTO for high power type.

2.2.2. Selection of three technologies (LTO, NMC, Li-S) and review of emblematic datasheets for each of them

The following paragraphs will detail current performances of the selected Li-ion technologies through some datasheets as well as forecasts coming from scientific publications and reviews.

2.2.2.1. Lithium Titanate Oxide anode based Lithium battery (LTO) – High Power

As mentioned previously, the LTO technology is a "High power" one, with very impressive C_{rate} capabilities (up to 10C continuous charge/discharge) and a very good cyclability (up to 20000 cycles). As LTO is used instead of graphite on the anode, the nominal cell voltage is usually around 2.3-2.4 V, which explains the relatively low specific energies (50-90 Wh/kg) compared to classic Li-ion cells. However, 100 % charge/discharge cycles are possible (contrary to the classical 80 % margin usually taken to preserve the battery from electrolyte degradation reactions) without degrading the performances. The high potential of the anode (1.5 V vs Li) limits the degradation mechanisms usually occurring with graphite anodes, allowing very good results in terms of cyclability even at high C_{rate}s. An illustration of these two aspects is visible on Figure 3 (from [TOS-17])) with discharge and cycling characteristics of a 20 Ah LTO cell developed by Toshiba (SCiB).

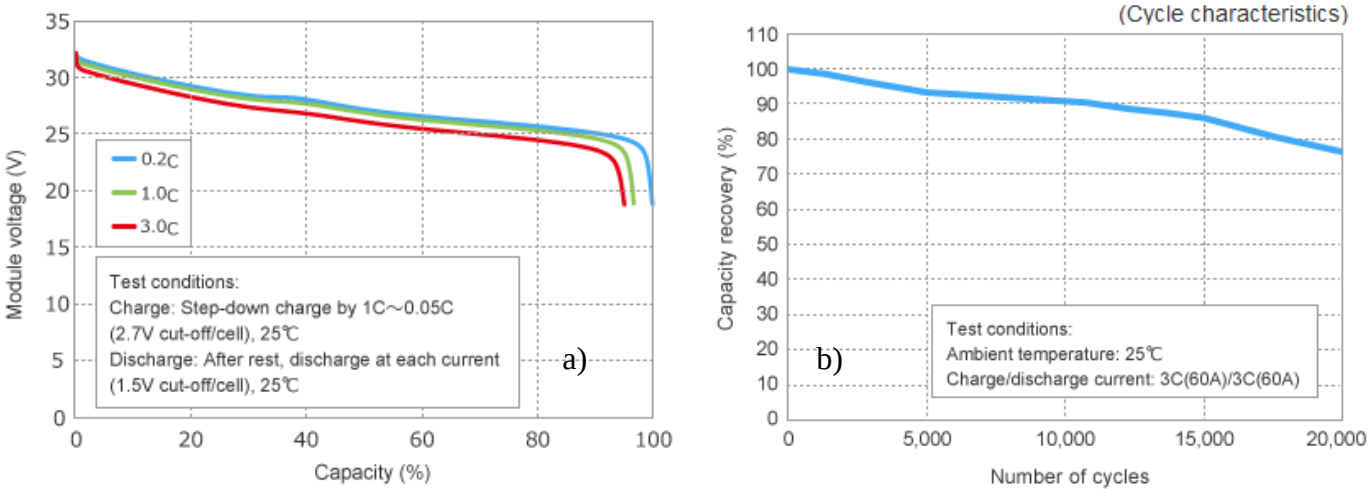

Figure 3 – a) Discharge curves characteristic of a SCiB Toshiba module 2P12S (20 Ah LTO cells); b) Cycling performances of a 20 Ah SCiB Toshiba cell at 3C/3C 100 % charge/discharge cycles ([TOS-17])

The "high power" aspect of this technology, issued from the spinel structure of the LTO anode which offer tunnels for fast Li ion mobility, is clearly highlighted here (Figure 3 a)): a high C_{rate} discharge is possible, and thus a high power output, without impacting much the available battery capacity and energy.

Table 2 synthetizes the current performances of three different manufacturers (Kokam, Leclanché and Toshiba) producing LTO cells and modules (the modules contain at least the packaging and BMS). The power capabilities are highlighted with the maximum possible continuous charge/discharge, at high rates such as 3C/4C in charge and discharge, here mentioned under the specific energies.

		Kokam ([KOK-14]	Leclanché ([LEC-14])	Toshiba SCiB ([TOS-17])
Cell type		Pouch	Pouch	Prismatic
Cell level	Wh/kg	77 Wh/kg	70-80 Wh/kg	47-96 Wh/kg
	Max continuous C_{rate}	4C charge / 8C discharge	3C / 3C	4C / 4C
	Wh/L	148 Wh/L (1.9 kg/L)	-	88-176 Wh/L (1.8 kg/L)
	Cycling life (20 % capacity loss)	20000 charge / discharge cycles at 1C and 80 % DOD	15000-20000 cycles at 4C and 100 % DOD	15000 cycles at 3C and 100 % DOD
System level (module)	Wh/kg	-	42 Wh/kg	78 Wh/kg
	Wh/L	-	46 Wh/L (1.1 kg/L)	128 Wh/L (1.6 kg/L)

Table 2 - Performances of current LTO technology at the cell and module level ([LEC-14], [KOK-15], [TOS-17])

A recent study ([TAK-18]) led by Toshiba, presents very impressive **perspectives** for this technology by changing the anode composition from LTO to mixed valency Ti-Nb oxide TNO ($TiNb_2O_7$) and thus increasing the specific capacity of the anode. The authors claims that the specific energy of this cell (TNO/NMC cell) can be improved to reach values such as 140 Wh/kg and 350 Wh/L, while keeping approximately the same C_{rate} and cyclability capabilities as LTO cells (up to 10C discharge and 14000 cycles at 100 % 1C charge/discharge cycles).

2.2.2.2. High Energy – Nickel Manganese Cobalt cathode based Lithium battery (NMC)

Unlike the LTO, the so-called NMC Li-ion battery refers to chemistries using NMC as cathode material and classically graphite for the anode material, allowing a higher cell voltage (hence a higher energy content) but also less power and cyclability capabilities (the high C_{rate}s charges/discharges are more impactful in terms of durability and degradations).

The aspects previously mentioned are clearly observable on Figure 4, where discharge curves as well as cycling characteristics are exposed for a Panasonic cylindrical NMC cell (ref UR18650ZTA, [PAN-18]).

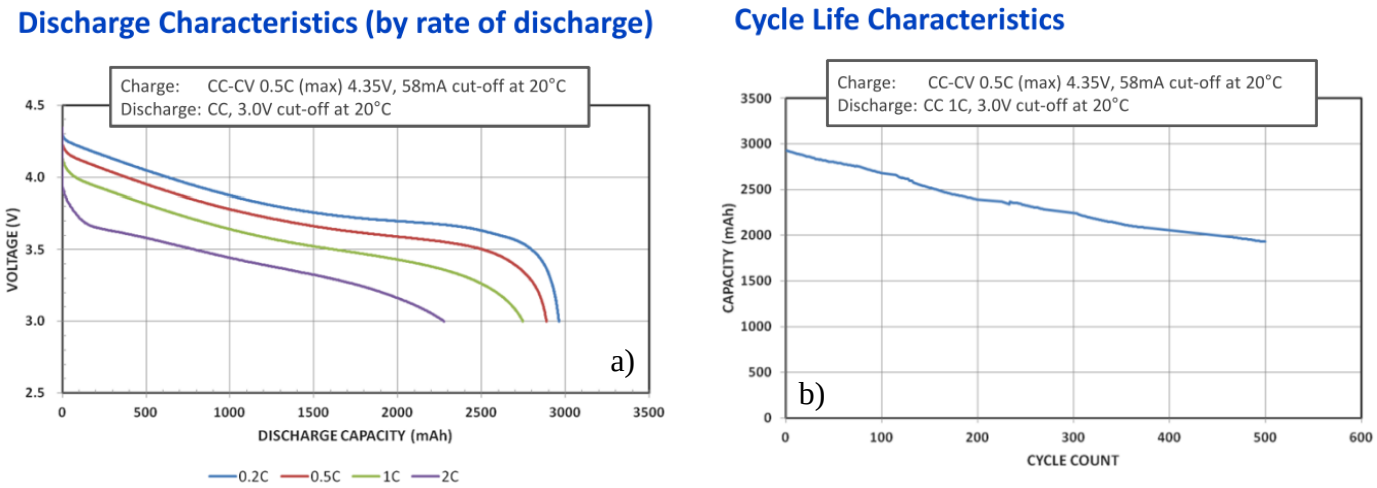

Figure 4 – a) Discharge curves characteristic of a Panasonic cylindrical cell (UR18650ZTA); b) Cycling performances of the Panasonic cell at 0.5C/1C charge/discharge cycles ([PAN-18])

If we compare Figure 4 and Figure 3, we can clearly see the different behavior of the high energy cell when increasing the C_{rate} compared to the high power one: the voltage curve is collapsing much faster when increasing the discharge current than with the LTO cell. If we look concretely the energy available for each discharge current, the actual specific energy at 2C is 158 Wh/kg vs 230 Wh/kg at 0.2C (32 % drop) for the Panasonic cell, while for the Toshiba cell the specific energy at 3C is 82 Wh/kg vs 90 Wh/kg at 0.2C (9 % drop). This little calculation underlines the relativity of the specific energy values: if the demanded power exceeds a certain value with respect to the energy contained inside the battery (the theoretical energy usually available at a low C_{rate}), the energy delivered will be lower than expected (depending on the battery technology). In other words, a single value associated to the specific energy cannot describe accurately the actual energy available in all situations, and depends on the C_{rate} at which the battery is used.

Several orders of magnitude have already been given previously (cf. Figure 2 and Table 1) for the high energy NMC cells (max 260 Wh/kg_{cell} and 150 Wh/kg_{system}). Table 3 presents, in order to give more concrete details, some key parameters of NMC cells from three different manufacturers (Kokam – Li-ion polymer cell, Leclanché, Panasonic) in terms of specific energies, C_{rate} limitations and cyclability. Through the observation of this table, we can see that even if some discrepancies are visible between the three cells, especially in terms of cyclability, the global specific energies reached, as well as the maximum continuous discharge rates, show good agreements between them (~ 200 Wh/kg and 2C max discharge). Despite the 18650 Panasonic cell ([PAN-18]) only have a poor cyclic life, LGchem 18650 NMC cell reach today more than 300 cycles with specific energies up to 260 Wh/kg_{cell}.

		Kokam ([KOK-15], [KOK-17])	Leclanché ([LEC-14], [LEC-14(2)])	Panasonic ([PAN-18])
Cell type		Pouch (Li-ion polymer)	Pouch	Cylindric
Cell level	Wh/kg	192 Wh/kg	120-200 Wh/kg	230 Wh/kg
	Max continuous C_{rate}	2C discharge (charge not precised)	2.3C (discharge) / 1C (charge)	2C (discharge) / 0.5C (charge)
	Wh/L	407 Wh/L (2.12 kg/L)	-	620 Wh/L (2.7 kg/L)
	Cycling life	-	8000 cycles at 80 % DOD (1C/1C)	20 % capacity loss after 200 cycles (33 % after 500 cycles)
System level (module)	Wh/kg	150 Wh/kg (@ C/2) (direct liquid cooling system included)	74 Wh/kg	-
	Wh/L	172 Wh/L (1.14 kg/L)	106 Wh/L (1.43 kg/L)	-

Table 3 – Performances of current NMC technology at the cell and module level ([LEC-14], [LEC-14(2)], [KOK-14], [KOK-17], [PAN-18])

In terms of prospects, one of the area of investigation is today focused on the **all solid-state technology with the use of a Li-metal anode** in order to increase the anode specific capacity, hence the cell specific energy. The key parameter linked with the change of the graphite anode to Li-metal is the constitution of the electrolyte ([SE-18]): it should be safe and not suffer from a lack of conductivity (which is the case of the polymer electrolytes, imposing high working temperatures precisely in order to increase their conductivity). Manufacturers such as Solid Energy ([SE-18]) or Sion Power ([SIO-18]) have already communicated about products presenting the same features (Li-metal/NMC cells with very high energy density). Sion Power is already announcing values such as 500 Wh/kg_{cell} and 1000 Wh/L_{cell} on their website with their Licerion® technology ([SIO-18]), but without giving complete information (no datasheet actually available).

However, Solid Energy has already published one datasheet (Hermès, [SE-18(2)]) detailing current performances of such type of cell with values up to 450 Wh/kg_{cell}, 1200 Wh/L_{cell}, 2C max continuous discharge and a working temperature range between -20 °C and 45 °C (complementary information is available on Appendix A). If we have a look on the datasheet published by Solid Energy (Appendix A), the main drawback seems to be the poor cyclability of the Li-metal/NMC cell: 10 % capacity loss after 100 cycles at 0.1C charge and 0.5C discharge. Another disadvantage of this technology should be as well its power capabilities for temperatures below 25 °C.

SSB (solid state batteries) will use polymer or ceramic solid electrolytes. Ceramic is the best route to follow in terms of safety. A target at 650 Wh/kg_{cell} should be reachable for 2035 if the

interface issues coming with the use of ceramic electrolyte and the Li anode and cathode (which in this case will both need coatings to stabilize the solid electrolyte) are solved, while using a bipolar design. There is today no guarantee that ceramic electrolyte-based SSB will come out, but many companies are working in this area. Finally, one thing to keep in mind is that ceramic-based SSB stacks will need to be kept under pressure to operate, to avoid loss of contacts between the electrode and the electrolyte, due to mechanical stress. This may affect the energy density. Another option is the use of solid polymer electrolytes to assemble SSBs. In this case, differently from the Blue Solution Lithium Metal Polymer battery, those polymers will operate at room temperature and below. This is highly challenging; however, it seems that a company (Ionic Materials) may have achieved a significant breakthrough in the field and raised > 100 US$ millions from big companies. However, to date, only plots are available and no detail on the chemistry has been disclosed. This company has to be tracked for the near future.

2.2.2.3. Lithium Sulfur battery (Li-S) – Very High Energy

The Li-S cells (also often featuring Li-metal anode) are very high energy cells, recurrently mentioned when forecasting the future of battery performances as the most promising in terms of energy density (cf. 2.2.1). However, there are nowadays few manufacturers producing Li-S cells and fewer Li-S battery racks or modules, hence it can be a bit delicate to assess the actual level of performances of this technology. In [BRU-12], the authors describe the main drawbacks of Li-S associated with each cell component: safety and cycling efficiency problems (linked to the Li-metal anode), limited rate capabilities and a poor volumetric efficiency (cf. Figure 5). Calendar aging can also be quite important according to [FRA-18] with non-negligible self-discharge effects.

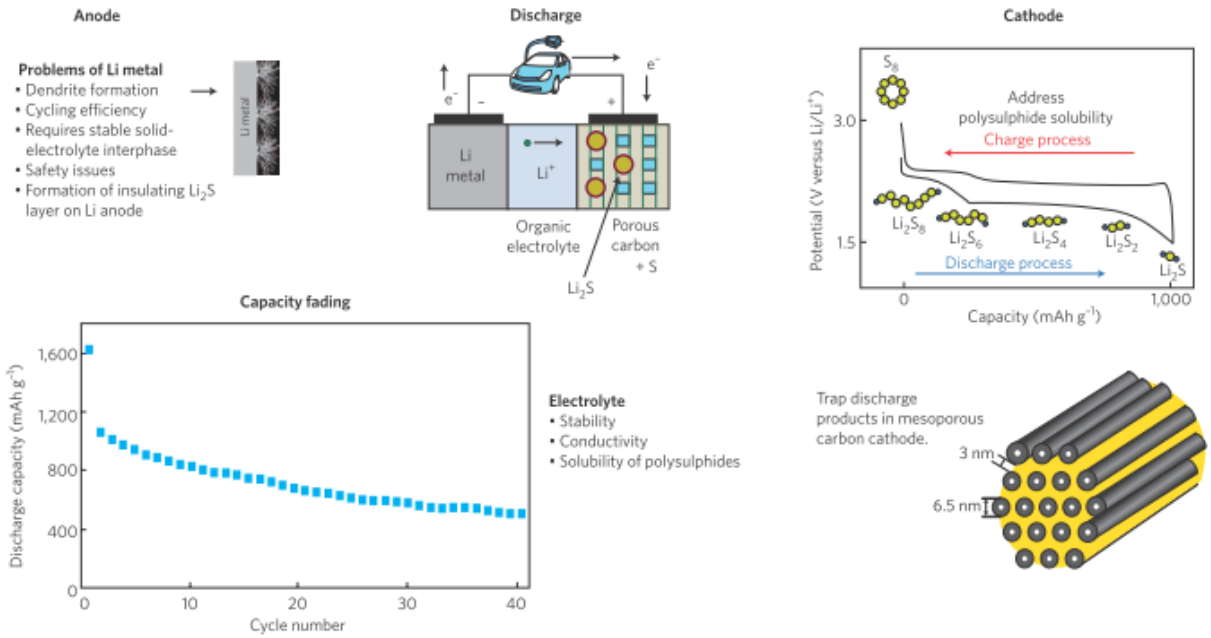

Figure 5 - Picture taken from [BRU-12] illustrating some issues faced by Li-S cells (rapid capacity loss, soluble sulfur as redox shuttles, electrolyte impedance behavior…)

Another study ([FOT-17]) corroborates the information given in [BRU-12] especially on the specific power limitations of this technology, underlining that above 1C, the specific capacity can drop dramatically.

Manufacturers such as Sion Power and Oxis Energy have already published some datasheet of Li-S cells ([SIO-08], [OXI-17]), whose main information are synthetized on Table 4.

Manufacturer	Oxis Energy (Appendix B) Pouch cell (POA0217)	Sion Power (Appendix C) Prismatic cell
Cell gravimetric energy	400 Wh/kg	350 Wh/kg
Cell volumetric energy	300 Wh/L (0.75 kg/L)	320 Wh/L (0.9 kg/L)
Cycling life (20 % capacity loss)	< 100 cycles at 80 % DOD	-

Table 4 - Main features of Lithium Sulfur cells developed by Oxis Energy and Sion Power ([SIO-08], [OXI-17])

Oxis Energy announces on his website that the target of 400 Wh/kg_{cell} has already been reached and that 500 Wh/kg_{cell} is on their roadmap for 2019. The company also manufactures currently Lithium Sulfur battery packs (datasheet available on Appendix B), reaching 120 Wh/kg and 73 Wh/L and reaching 1400 cycles at 80 % DOD for a capacity loss of 40 %.

In terms of **prospects**, the manufacturer projection already mentioned ([OXI-17]) target 500 Wh/kg_{cell} / 500 Wh/L_{cell} with improved cyclability (1000 cycles at 80 % DOD) for 2019 (cf. Appendix B). Other forecasts for this technology with a longer-term horizon have already been exposed in Table 1 (values taken from [FUS-15]).

2.2.3. Overview of the battery weight integrating factor values assessed in the literature

Without having much specification on a concrete integration case, it is quite difficult to make an accurate estimation of the weight impact of the different components necessary to make the step from the cell to the battery system. Nevertheless, a rough estimation can be made using a simple formula with a weight integrating factor f_m:

$$m_{system} = m_{cell} * f_m \quad (2)$$

Several orders of magnitude for this weight impact can already be deducted from the previous tables when going from the cell level line to the system line (cf. Table 2 and Table 3). However the "system" level mentioned can refer to different set of components (cells, connections, packaging, BMS, cooling system) and the cells used to make the packs are not necessarily the exact cells mentioned on the upper line (cell level), so the estimation of the auxiliary components weight impact through this way can be rather uncertain.

A few articles and publications quantifying this weight impact when passing from the cell level to the system level (adding the connections, sensors, cables, BMS, cooling system and packaging) have been reviewed and are synthetized on Table 5.

Considering the values referenced in this table as well as the aeronautical context of the study, the upper limit of $f_m = 2$ is taken as reference in order to estimate the weight impact factor of the packaging, BMS and cooling mass.

Looking the volume impact on the system integration (parameter f_v), there is unfortunately fewer information in the studies quoted in Table 5 than for the weight impact: from [FUS-15] it appears that this parameter is apparently higher with values up to 2.5 – 3. It must be precised here that, being rigorous, the f_m and f_v factors should depend on parameters such as the battery technology employed, the cell type (pouch, prismatic or cylindrical) or the power mission profile and temperature conditions for instance.

The final assumptions made on the specific energies / powers / cycling life corresponding to the previously mentioned technologies (current performances and forecast) are exposed in a synthetic way in the 2.4 section.

Reference	Weight integrating factor (f_m) estimation	Comments
[PER-18]	1.4	Cell to pack
[BIR-10]	1.43	Automotive context – mild-hybrid – Cell to system (including cooling)
LG chemistry pack (Zoé/Renault)	1.8	Cell to system (automotive context)
[MUE-18]	1.43	Cell to system (future aeronautical context assessment)
[TAR-16]	2	Cell to system (charger, casing, sensing circuitry) – aeronautical context
[STU-12]	2	Cell to system (including cooling and BMS) – aeronautical context
[FUS-15]	1.6 – 2	Cell to system – aeronautical context

Table 5 - Non-exhaustive overview of weight integrating factor assessments in different studies

2.3. State of the art of FC stacks and systems power densities and H_2 storage systems energy densities for mobile applications (automotive and aeronautical)

After having detailed in the previous part a state of the art of the current performances of several battery technologies, the next paragraphs will focus on the Fuel Cell performances and on their associated H_2 storage systems.

The objective of this section is, as well as for the battery part, to collect relevant orders of magnitude of the current and future performances of such devices in terms of power densities, weight impact of the fuel cell auxiliaries and H_2 storage gravimetric/volumetric efficiencies.

2.3.1. *Pre-selection of the FC technologies and H_2 storage methods*

In an attempt to limit the potential technologies considered, a first selection of the fuel cell technologies has been made and is summarized Table 6.

Fuel Cell technologies considered		
Low Temperature Proton Exchange Membrane Fuel Cell (LT PEM FC) Temperature: ~ 60 – 80 °C	High Temperature Proton Exchange Membrane Fuel Cell (HT PEM FC) Temp.: ~ 140 – 180 °C	Solid Oxide Fuel Cell (SOFC) Temp.: ~ 600 – 1000 °C

Table 6 – List of the pre-selected Fuel Cell technologies

Among the three FC technologies, the Low Temperature PEM FC is the most mature one (industrially speaking) and the most popularized in markets such as the automotive market, with products currently commercialized and available such as the Honda Clarity or the Toyota Mirai ([YOS-15], [MAT-09]).

The High Temperature PEMFC and SOFC present both less maturity than the LT PEMFC and show for most of them lower power conversion efficiencies at the stack scale (~ 0.5 at 0.2 A/cm² vs 0.5 at 1-1.5 A/cm² for the LT PEMFC). Nevertheless, other advantages linked to their working temperatures can make their integration easier in several contexts. The HT PEMFC does not need any humidification system for instance, whereas LT PEMFC stacks usually need it in order to monitor the cell's membranes hydration level. In a similar vein, contrary to the LT PEMFC, the very high working temperature of the SOFC allows several possibilities for the system implementation (like coupling with gas turbines) as well as a higher tolerance to contaminants or other fuel mix.

Regarding the energy storage, H_2 storage methods are also pre-selected (Table 7):

H_2 storage technologies considered		
Compressed H_2 (350 bara and 700 bara) composite tanks	Liquid H_2 cryogenic tanks (20 K)	Solid H_2 storage (metal hydrides)

Table 7 – List of the pre-selected H_2 storage technologies considered

2.3.2. *State of the Art of the FC stack and system power densities: High Temperature / Low Temperature PEM FC and Solid Oxide FC*

Due to the abundance of available information in the literature on current LT PEMFC performances on one hand and to the lack of information on current HT PEMFC and SOFC performances on the other hand, the following parts will mainly focus on the LT PEMFC. As a matter of fact, most studies on HT PEMFC and SOFC systems are focused on future integration concepts and rarely give some insights into their concrete performances in terms of global power densities at the stack and system scale. Also, the FC system power densities mentioned in the next paragraphs is related to the **power conversion part only (FC stacks and auxiliaries)** and does not account for the H_2 storage mass or volume.

2.3.2.1. Low Temperature Proton Exchange Membrane FC (LT PEMFC)

A lot of developments and improvements on LT PEMFC stacks and systems have already been done to this day, mainly driven by the automotive industry for the embedded applications. The DOE (Department of Energy) is actually fixing the global targets for the embedded applications accordingly to the automotive systems requirements where, for instance, the stack gravimetric power density target of 2 kW/kg for 2020 ([DOE-16]) is already reached and the volumetric power density target of 2.5 kW/L is well surpassed as well since 2014 ([YOS-15]).

Figure 6 illustrates the development tendency of Toyota LT PEMFC stacks from 2002 to 2017 as well as the volumetric and gravimetric DoE targets marked with green doted lines.

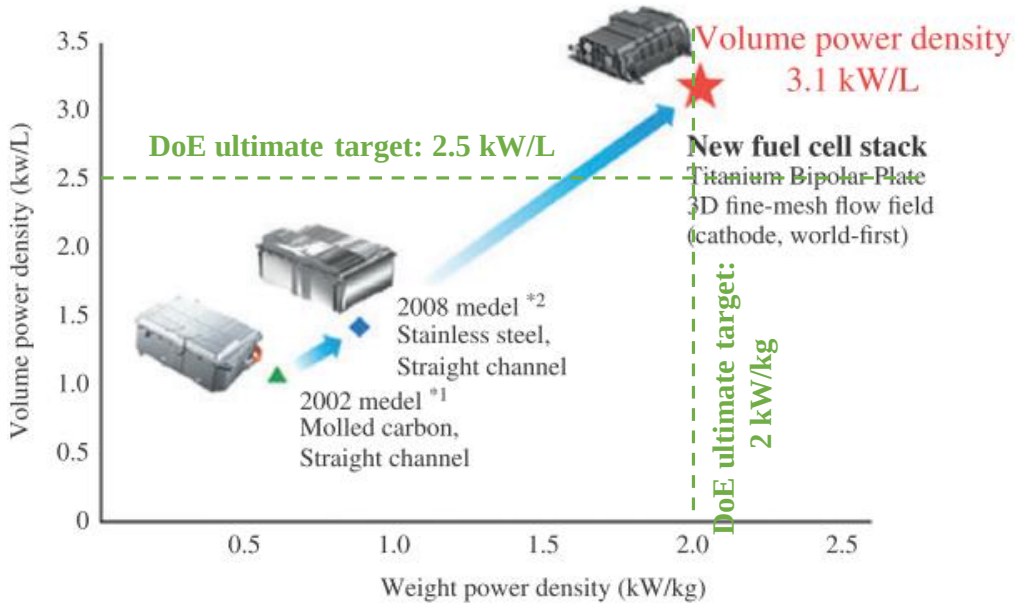

Figure 6 - Past and current performances of Toyota LT PEMFC stacks (power densities), [NON-17] - Ultimate targets of the DoE for transportation FC stacks (in green), [DOE-16]

FC systems usually feature some Balance of Plants (BoP) components (also called auxiliary components or simply auxiliaries) providing to the FC stack appropriated environmental conditions to work properly (air and H_2 supply and fluidic management, thermal control, humidity control…).

Between all these auxiliary components, a few can be mentioned without being exhaustive:

- An air delivery unit usually featuring an air compressor, a regulator and an appropriate circuitry (tubes, pipes)
- A hydrogen fluidic control system (pressure and flow); it can be with or without any recirculator unit
- A humidification system in order to monitor the stack's cells hydration
- A cooling system to monitor the stack working temperature (depending on the cooling method, it can feature a condenser, radiators, a cooling pump, tubes, valves…).

Although, as we will observe later, not all these BoP components are necessarily presents in all the FC systems, they can appear regularly depending on the constructor and the environmental constraints. An illustrative example of a FC system is proposed on Figure 7 to highlight the different loops and circuits (air, H_2 and cooling) as well as the auxiliary components surrounding a FC stack. In this automotive example (Toyota Mirai case, [KOJ-15]), the humidification system is for instance eliminated thanks to several improvements at the cell scale (very thin membranes enhancing the water crossover) and on the H_2 recirculation system, allowing an efficient self-humidification and internal water loop inside the stack ([HAS-16]).

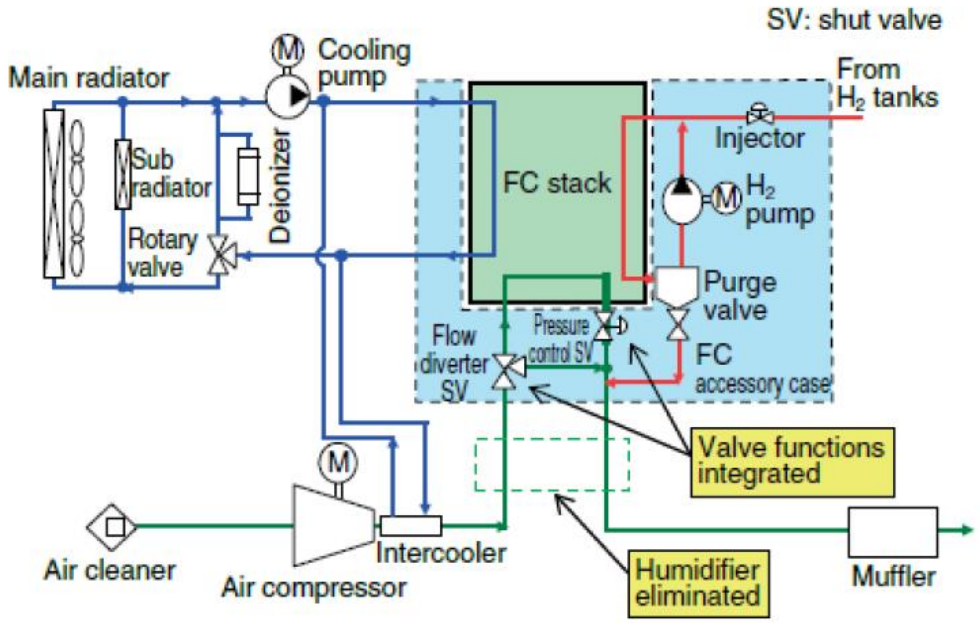

Figure 7 - Illustrative example of a FC system in an automotive embedded case (Toyota Mirai) - Picture taken from [KOJ-15]

As all the auxiliary components are not passive elements, some will consume a parasitic part of the whole power generated by the FC stack to work properly (mainly the air compressor). Based on this observation, a distinction can be made between the power generated by the FC stack, the gross power (P_{gross}), and the power delivered by the FC system, the net power (P_{net}), which is the actual usable power after considering the auxiliary parasitic power consumption (P_{aux}) as described on eq. (3).

$$P_{net} = P_{gross} - P_{aux} \quad (3)$$

As mentioned previously, automotive constructors such as Honda, General Motors or Hyundai already commercialize FC electrical vehicles comprising a fuel cell stack, stack auxiliaries like a cooling loop with a radiator, and a compressed H_2 storage unit (700 bara composite tanks). Furthermore, a few manufacturers, such as Ballard, Hydrogenics, Intelligent Energy or PowerCell between others, propose mature products (stacks and systems) for high power mobility applications (cars, busses, boats…).

In an attempt to reference the performances of such devices, Table 8 summarizes some data in terms of power densities at the stack and system scale published by these different manufacturers or visible in scientific publications. For the sake of simplicity, and in order to consider numbers at a power scale relatively close to the one of the auxiliary mission (a few hundreds of kW), only high power stacks and systems are mentioned. As it can be seen in this table, it is sometimes delicate to associate values at the stack and at the system scale: some information are often given in an incomplete manner (a stack power density without the corresponding system power density for instance).

Moreover, the FC "system" appellation is often quite ambiguous and can lead to several misunderstandings: quite often, the so called FC system will feature a FC stack and some auxiliary components but not all of them. For instance, the cooling system mentioned in some modules will often be incomplete and won't include the external radiator; hence, one can underestimate the global weight and volume of the actual system while thinking the global cooling loop mass and volume are considered.

Nevertheless the comparison of these numbers, especially for the last lines of Table 8, highlight quite impressively the actual impact of the transition from the stack scale to the system scale regarding the power density. The data from [POW-16(1)], [POW-16(2)] and [IE-15] allow a fair comparison of the performances before and after the integration of the stack into a system and show a huge impact for this integration (from 2.9 kW/kg to 0.74 kW/kg for the PowerCell stack and system for instance). Regarding the system description, the module presented by Intelligent Energy on the last line of the table (Appendix D) is the most complete one (the mass and volume information contain all the auxiliary components, including the condenser in the cooling unit). For this module, the specific power drops from 3 to 0.667 kW/kg (0.22 factor) when jumping from the stack to the system scale.

The decrease in power density from the FC stack to the FC system scale can be explained not only by the weight impact of the auxiliaries but also by their parasitic power consumption decreasing the overall power available, which is highlighted in eq. (3), (4) and (5).

$$p_m^{gross/FC}\left(\frac{kW}{kg}\right) = \frac{P_{FC}(= P_{gross})}{m_{FC}} \tag{4}$$

$$p_m^{net/system}\left(\frac{kW}{kg}\right) = \frac{P_{system}(= P_{net})}{m_{system}} = \frac{P_{FC} - \boldsymbol{P_{aux}}}{m_{FC} + \boldsymbol{m_{aux}}} \ll p_m^{gross} \tag{5}$$

With $p_m^{gross/FC}$ and $p_m^{net/system}$ being respectively the gravimetric power densities at the FC stack and at the system scale, and m_{FC}, m_{aux} and m_{system} respectively the FC stack, auxiliaries and system masses.

Hence, the challenge in terms of system power density increase does not only rely on lighter auxiliaries but as well on minimizing their power consumption.

Reference	Power densities (gravimetric – p_m – and volumetric – p_v)		Comments / remarks
	Stack scale	System scale	
[HYD-16]	-	0.430 kW/kg (p_m)	Hydrogenics HD-30 module with complete BoP components (~ 30 kW_{net}). p_m value: without coolant pump mass. p_v value: without coolant pump and air delivery volume.
	-	0.410 kW/L (p_v)	
[HYD-16]	-	0.275 kW/kg	Hydrogenics HD-180 module (~ **200 kW_{net}**). p_m and p_v assessments without some BoP components (cf. HD-30 module – upper line).
	-	0.167 kW/L	
[BAL-16]	> 0.350 kW/kg	0.256 kW/kg	Ballard FCveloCity Heavy-Duty module HD-100 (~ **100 kW_{net}**). Assessments of p_m and p_v at the system scale consider the FC module plus the air and cooling subsystems (normally deliberately dissociated to improve the system flexibility).
	> 0.190 kW/L	0.130 kW/L	
[FON-13]	-	0.434 kW/kg	CEA estimation for automotive embedded FC systems (including stack, auxiliaries and connections).
[MAT-09]	1.5 kW/kg	-	Honda FCX Clarity (2009) Fuel Cell stack (~ **100 kW_{gross}**) power densities.
	2 kW/L	-	
[NON-17], [ESA-18]	2 kW/kg	~ 0.7 kW/kg	Toyota Mirai (2014) Fuel Cell stack (~ **114 kW_{gross}**) power densities. Assessment at the system scale by ESA.
	3.1 kW/L	-	
[POW-16(1)], [POW-16(2)]	2.91 kW/kg	0.740 kW/kg	PowerCell S3 FC stack (~ **125 kW_{gross}**) and MS 100 (~ **100 kW_{net}**) FC system. Assessments of p_m and p_v values are made without considering the external radiator (liquid cooling) and the air filter.
	3.37 kW/L	0.333 kW/L	
[IE-15] (Appendix D)	3 kW/kg	0.667 kW/kg	Intelligent Energy Evaporative Cooling automotive Fuel Cell system (~ **100 kW_{net}**). Assessments of p_m and p_v values are made considering complete BoP components, including the condenser radiator, the air delivery system (with the compressor)…
	3.5 kW/L	0.595 kW/L	

Table 8 – Overview of LT PEMFC stacks and systems performances in terms of power densities: p_m and p_v (highlighted with a blue background)

Prospects regarding LT PEMFC power densities:

In terms of prospects, many improvements have already been done at the stack scale (cf. Figure 6) with a doubling of the stack power density in less than 10 years.

As can be seen in Table 8, power densities of around 3 kW/kg are already achieved ([IE-15]), by changing the stack traditional architecture and the stack cooling system. More precisely, as the stack is evaporatively cooled with the direct injection of liquid water in the cathode compartments of the stack's cells, there are no cooling channels neither cooling plates usually used with classic direct cooling structures. Very thin single piece bipolar plates can then be employed ([IE-18]) and further reduction of the overall stack weight can be achieved, increasing the power density. Such method can pave the way to future weight reductions of LT PEMFC stacks and bring even higher power densities.

Moreover, in order to reach the target of 2 kW/kg (previous model reached 0.83 kW/kg – [KOJ-15]), Toyota ([NON-17]) achieved an increase of the stack areal power density (W/cm²) by a factor of 2.3 by boosting the catalyst activity and using revolutionary air channels structures (3D fine-mesh flow field structure), together with a reduction of some of the stack constitutive material (20 % thinner membranes) and the use of titanium for the bipolar plates (weight reduction by almost 40 %).

According to [HAS-15] (Nissan research center), future performances of LT PEMFC stacks could reach in the short-term (2025) a target of around 5 kW/kg and 8.5 kW/kg in the mid-term (2030-2035) with improvements focusing on, on one hand increasing the areal current densities (up to 2 to 3 A/cm²), and on the other hand decreasing the cell pitch (enhancing more in this case the volumetric power density).

Kadyk et al. ([KAD-18]), exploring potential FC systems for aviation, assert that power densities up to 10 kW/kg at the stack level could be reached in the future by the same means described in [HAS-15] and [NON-17] (changing the graphite bipolar plates for metallic ones with carbon coating in order to avoid corrosion on one hand and increasing the areal power density on the other hand), with 8 kW/kg at the system level.

2.3.2.2. Weight impact of the auxiliaries

As mentioned earlier, the auxiliaries have a double weight impact on the overall system power density: because they add a burden to the system and because they consume a part of the power generated by the FC stack. If the parasitic power consumption of such components can be estimated looking to the system efficiency, it is sometimes delicate to find a direct reference to their masses in the previous sources quoted Table 8.

Several publications such as [HAS-15] estimate approximately the total mass of the auxiliary components proportionally to the FC stack mass with a range between 100 and 300 % of the FC stack mass, while others simply estimate empirically the auxiliary weight proportionally to the FC stack gross power ([POG-18]).

Regarding the two ways of assessing the weight of the auxiliary components (proportionally to the stack mass or to the FC stack power), the second one seems the most appropriate since the mass of the auxiliaries mainly depends on their own parasitic power consumption or on the FC stack heat to evacuate. Indeed, the air compressor for instance will be designed regarding its pressure conversion ratio and its airflow rate, while in return this airflow rate should be proportional to the FC stack power generation and efficiency. Considering a fixed efficiency on the design point, the compressor size (hence its mass and volume) will thus mainly depend on the FC gross power. The same argument can be applied to the Hydrogen recirculation pump. Moreover, the cooling system size will depend (all the environmental conditions being fixed) on the heat generated by the stack which is proportional to the FC stack power and to its efficiency. In the end, even if the approximation is not completely rigorous, we make the hypothesis that the auxiliary mass is directly proportional to the FC stack gross power. An empirical parameter called the auxiliaries specific weight impact, p_m^{aux} (p_v^{aux} in its volumetric declination), is thus introduced to highlight this link (equation (6)).

$$p_m^{aux}\left(\frac{kW}{kg}\right) = \frac{P_{FC}(= P_{gross})}{m_{aux}} \tag{6}$$

The parameter is homogeneous to a gravimetric specific power even if in this case the power mentioned is obviously not coming from the auxiliary components but from the FC stack.

If we take back the equation (5), the system specific power p_m^{system} can now be reformulated this way:

$$p_m^{system} = \frac{P_{net}}{m_{FC} + m_{aux}} = \frac{P_{net}}{P_{FC}} * \frac{1}{\frac{m_{FC}}{P_{FC}} + \frac{m_{aux}}{P_{FC}}} \tag{7}$$

$$p_m^{system} = \frac{P_{net}}{P_{FC}} * \frac{1}{\frac{1}{\boldsymbol{p_m^{FC}}} + \frac{1}{\boldsymbol{p_m^{aux}}}} \tag{8}$$

Looking the equation (8), we see that we can link together p_m^{system}, p_m^{FC} and p_m^{aux} which are only power coefficients between them, if we can estimate the P_{net}/P_{gross} ratio. If these information are not available, the ratio can be estimated from the FC stack and system power conversion efficiencies respectively η_{FC}^{stack} and η_{FC}^{system} as developed in equations (9), (10), (11).

$$\eta_{FC}^{stack} = \frac{P_{FC}}{P_{H2}(= \dot{m}_{H2}^{in} * LHV)} \tag{9}$$

$$\eta_{FC}^{system} = \frac{P_{net}}{P_{H2}} \tag{10}$$

$$\frac{P_{net}}{P_{gross}} = \frac{\eta_{FC}^{system}}{\eta_{FC}^{stack}} \tag{11}$$

With LHV the Lower Heating Value of H_2 (33.3 kWh/kg), $\dot{m}_{H2}^{in}$ the hydrogen input mass flow (kg/h) and P_{H2} the hydrogen chemical power (kW). Knowing either the gross and net power, either the FC stack and FC system power conversion efficiencies, p_m^{aux} can be deduced from $p_m^{system}$and p_m^{FC}. Interestingly, these information are given one way or another for the three FC systems given in the last lines of Table 8:

- For the Toyota Mirai FC system, the efficiencies η_{FC}^{stack} and η_{FC}^{system} at maximum power are already known from [LOH-17] (respectively 0.5 and 0.42), as well as p_m^{system}(ESA estimation, [ESA-18]) and p_m^{FC} ([NON-17]).
- For the PowerCell S3 high power stack and MS 100 FC system ([POW-16(1)], [POW-16(2)]), the stack polarization curve is available allowing a close estimation of the FC stack conversion efficiency η_{FC}^{stack} around 0.55 at full power. The system global efficiency at full power (η_{FC}^{system} = 0.5) is also given.
- For the Intelligent Energy module (Appendix D), the system global efficiency is given as well (0.4). A hypothesis on the FC stack efficiency (η_{FC}^{stack} = 0.5) is made to complete the picture.

Additionally, based on experimental data from the Hy4 small airplane (using LT PEMFC stacks – 4 stacks at 45 kW each – and a Li-ion battery for the propulsion system [Hy4]), an estimation of the auxiliary components mass is given by [POG-18] for a 150 kW_{gross} / 133.5 kW_{net} FC system: an estimation of p_m^{aux}, moreover in an aeronautical context, can then be made. Also, some values of p_m^{FC} and p_m^{system} can be assessed from [POG-18] and compared to the ones already mentioned Table 9: p_m^{FC} = 2 kW/kg and p_m^{system} = 0.731 kW/kg.

A final overview of the values of p_m^{aux} (and p_v^{aux} when possible) estimated for these four sources is given Figure 8. As it can be seen, the estimations show globally a good agreement between them despite the systems have different scales and are designed for different operation (Toyota Mirai vs Hy4 for instance) with values around 1.13 and 1.43 kW/kg for the auxiliaries gravimetric impact p_m^{aux}. Due to the lack of information, it is however more delicate to assess coherent values for the auxiliary volumetric impact p_v^{aux}: the two values estimated (0.41 and 0.94 kW/L) show great difference. In this case, the evaluation of p_v^{aux} for the Intelligent Energy module (0.94 kW/L) should be more reliable than the one made for the MS 100 PowerCell FC system because the IE module features absolutely all BoP components.

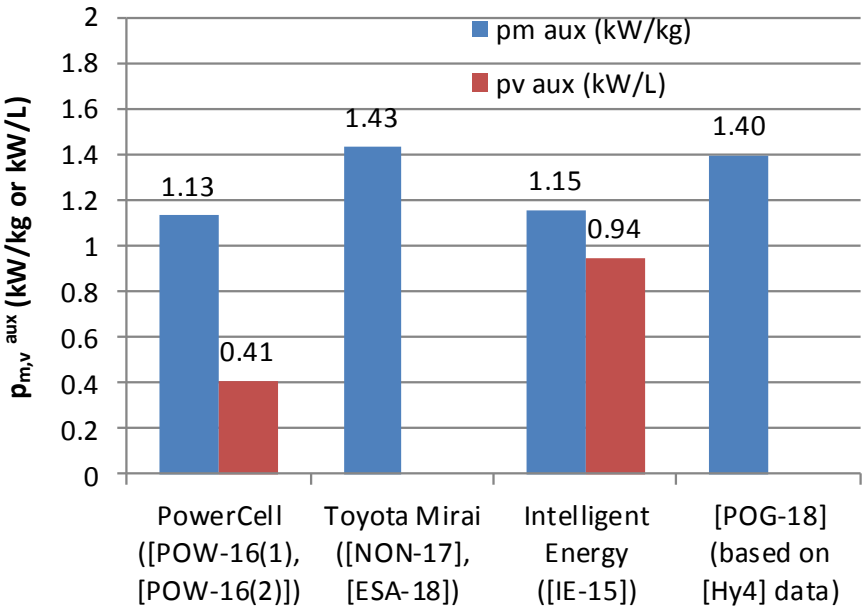

Figure 8 - Summary of the estimated value of p_m^{aux} (kW/kg) in blue and p_v^{aux} (kW/L) in red

2.3.2.3. High Temperature PEM FC and Solid Oxide FC

As discussed in the introduction of the 2.3.2, due to the lack of maturity of the HT PEMFC and the SOFC compared to the LT PEMFC it is quite delicate to assess their actual level of performances. This being said, a few studies presenting HT PEMFC or SOFC system concepts or even demonstrations for transport applications ([EEL-04], [REN-16]) have already been published underlining the potential advantages of such technologies in various contexts. Mainly because of their high working temperatures, they inherently present easier integration aspects with respect to their cooling system ([ROS-17]), as well as a better tolerance to contaminants (such as CO for instance). On the other hand, their high working temperature (especially for the SOFC), bring as well some constraints in terms of start-up time: the temperature raise from the ambient temperature to the operating temperature should not be too quick in order to minimize the mechanical stresses inside the stack in the SOFC case for example.

In [REN-16], the authors present a 1 kW HT PEMFC stack designed for a high altitude operation (10 km) in an UAV (Unmanned Aerial Vehicle) with an appropriate air cooling system. Their stack reaches a power gravimetric density of about **0.3 kW/kg** at its maximum power point and around 0.16 kW/kg at the FC system scale which is, at least for this example, highlighting a great gap between LT and HT PEM FC performances at the moment. However, in [NEO-17], the authors claim to have reached a maximum gravimetric power density of about **0.8 kW/kg** with a 5 kW HT PEMFC stack designed for a telecom satellite.

Regarding the SOFC, in [EEL-04], [RAJ-08], [MIS-18], concepts for the hybrid electric propulsion or for the Auxiliary Power Unit (APU) in an aeronautical context are presented, and interesting trade-offs between SOFC systems and Gas Turbines are shown (an example of potential benefits resulting from such an association for the APU is shown Figure 9). In this

case ([RAJ-08]), a fuel reformer is used to feed the SOFC and the products of the SOFC (high temperature exhaust air and syngas) are further reemployed in a Gas Turbine. As the global system energetic efficiency is improved compared to the use of a gas turbine, the global fuel consumption is reduced, but in return the target presented in terms of system gravimetric power density should be > 0.5 kW/kg for the entire SOFC system. Regarding the estimation of the SOFC gravimetric power density, [ROT-10] gives an estimation for the current performances around **0.33 kW/kg** which is, at least for the previous study case ([RAJ-08]), rather pessimistic.

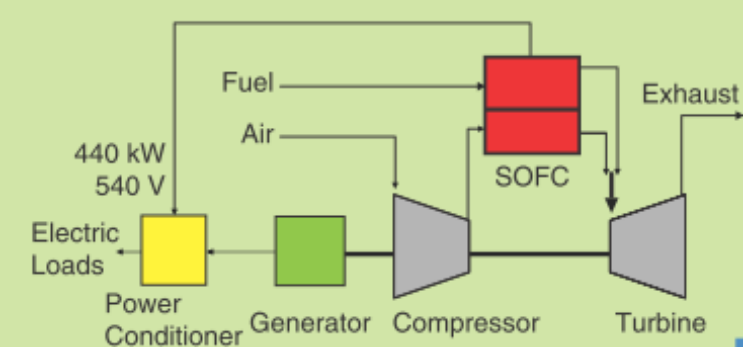

Figure 9 - Simplified example of a SOFC-GT concept for the APU (picture taken from [RAJ-08])

In conclusion, even if concepts of HT PEMFC and SOFC systems in the aeronautical context seem to be promising (HT PEMFC in the mid-term and SOFC in the long-term), it is still quite delicate to assess the actual level of performances of such technologies due to the lack of maturity and feedback from current system performances. The only few values of present gravimetric power density of HT PEMFC or SOFC stacks observed in the different articles reviewed, seem for the moment way behind LT PEMFC ones. At the system scale, clear benefits could appear in terms of implementation in an airplane when using such technologies, but again hardly quantifiable regarding their current level of maturity.

2.3.3. Overview of the gravimetric and volumetric performances of the H_2 storage methods

After a focus on the evaluation of current and future FC stack and system performances, this part is going to deal with the energy storage brick, i.e. the H_2 storage methods. As detailed in Table 7, three storage methods are considered: compressed H_2 composite tanks, liquefied H_2 tanks and metal hydrides.

2.3.3.1. Compressed H_2 tanks

Between all the H_2 media storages, composite tanks containing compressed H_2 are among the preferential options in the automotive industry (option chosen – 700 bara tanks – for the Toyota Mirai or the Honda Clarity between others), because of their lightness and reduced volume. Such type of H_2 storage has quite improved its gravimetric performances during the past years: an increase of the gravimetric efficiency from 4.6 wt. % to 5.7 wt. % between 2008 and 2014 has for instance been achieved with 700 bara composite tanks by Toyota (the value of 5.7 wt. % is a world record in 2014, [NON-17]). The H_2 volumetric capacity of these

current composite tanks of the Toyota Mirai is around 0.041 kg_{H2}/L. In terms of energy density, such tanks would thus reach about 1.88 kWh/kg and 1.35 kWh/L considering the LHV of hydrogen (without taking into account the efficiency of the energy converter i.e. the Fuel Cell). In small aerial vehicles, such storage systems have already been used ([Hy4], [REN-16]) coupled with a FC, but with lower storage pressures.

Indeed, depending on the tank pressure, the two values (gravimetric efficiency and H_2 volumetric capacity) can vary in a non-negligible way. Using as reference products from Hexagon Composite (compressed H_2 storage composite tanks manufacturer) in [HEX-17], one can see the evolution of these two parameters depending on the storage pressure in Figure 10.

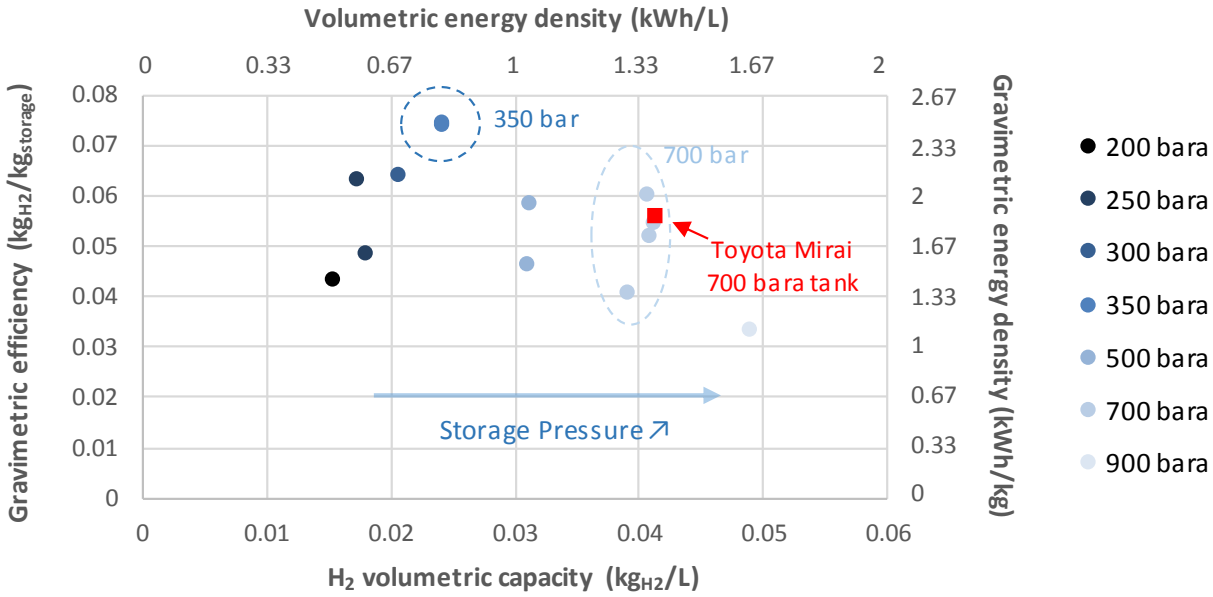

Figure 10 - Gravimetric and volumetric performances of composite storage tanks (type IV) containing compressed H_2 (data from Hexagon Composite manufacturer, [HEX-17])

Obviously, when the storage pressure increases, the H_2 volumetric capacity increases as well: a maximum of 0.05 kg_{H2}/L is almost reached at 900 bara. However, there are no gain visible (at least for this data) after 350 bara regarding the gravimetric efficiency: moreover the gravimetric efficiencies drop after 350 bara (where a maximum of 7.5 wt. % is reached).

With respect to the energetic cost of the H_2 compression operation, a multi-stage 700 bara compression would require around 4.5 kWh/kg_{H2} while 3.3 kWh/kg_{H2} would be used for a 350 bara compression ([MAK-17]). This values represent respectively 13 % and 10 % of the LHV of hydrogen, which should be kept in mind when considering the overall energy balance.

Although tanks of compressed H_2 are an attractive option for the energy storage (taking into account its maturity, lightness and energy density), it should be kept in mind that putting high-pressure tanks in an airplane is a high challenge in terms of compliance to the specific aeronautic safety requirements.

2.3.3.2.Liquid H_2 tanks

Due to its intrinsic properties, H_2 in its liquid form (LH_2) presents obvious advantages in terms of energy density (70.9 kg/m^3 – 2.34 kWh/L – at 1 atm and ~ 20K) compared to compressed H_2. When looking to its gravimetric and volumetric energy capabilities with respect to kerosene, one can see that while LH_2 present a higher gravimetric energy density (33.3 kWh/kg vs 12 kWh/kg for kerosene), its volumetric energy density is much less than the kerosene one (respectively 2.34 kWh/L vs 9.7 kWh/L). The Figure 11 highlights the proportion differences in mass and volume for the same energy content between LH_2 and kerosene to illustrate these aspects.

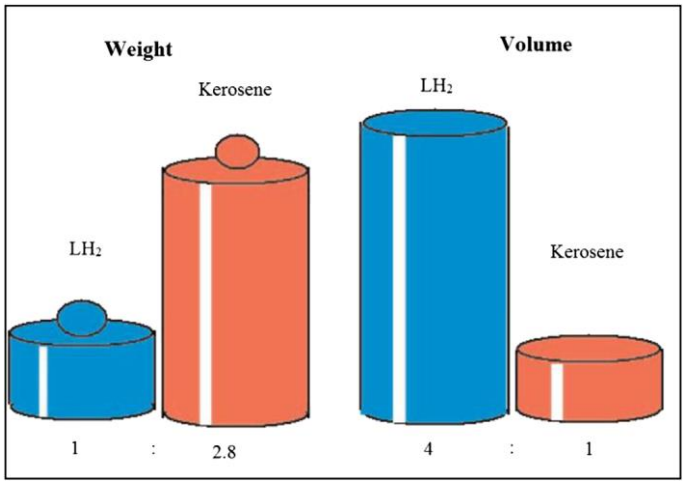

Figure 11 - LH_2 and Kerosene weight and volume comparison for a given energy content ([NOJ-09])

To make a fair comparison in terms of gravimetric and volumetric energy densities between the two elements (LH_2 and kerosene), one should nevertheless consider the impact of the tank weight and volume on the energy storage system (higher in the case of LH_2 than for kerosene, [WIN-18]). Such comparison between kerosene and LH_2 is made in studies such as [WES-03] (Cryoplane project), [HAG-06], [VER-10], [KHA-13], when considering LH_2 as a potential candidate to replace kerosene in direct combustion engines for aviation applications.

In [VER-10] and [WIN-18] in particular, the authors investigate potential LH_2 tank designs for aviation applications (regional airliner) by taking into account various parameters such as the tank geometrical shape, the H_2 venting pressure inside the tank (maximal acceptable H_2 pressure before venting), the insulation type (between other factors). Such tanks generally feature a double-wall structure (inner and outer wall) with an insulating layer between the two walls, as well as a venting pipe and a filling pipe. Regarding the insulation methods to maintain the ~ 20 K necessary to keep the H_2 in liquid state and limit the boil-off of LH_2, three possibilities are often mentioned ([KHA-13], [VER-10]):

- A Multi-Layer Insulation (MLI), consisting of a superposition of metallic foils and insulating thin material (polyester or glass fiber for instance) to avoid metal-to-metal contact. The MLI insulation should act as a shield for the thermal radiations ([KHA-13]), however the layer density should not be too high in order not to increase the conduction

effects between the two walls. To minimize gas conduction, MLI has to operate at ~ 12 mbar pressures ([VER-10]).

- A vacuum insulation: while [KHA-13] underlines that it is theoretically the best option, the authors add that it is practically impossible to maintain a vacuum without additional venting equipment (pumps to suck the air and maintain the vacuum).
- A foam insulation, consisting of a foam layer put between the two walls. As the thermal conductivity of such foams is higher than the MLI under very low pressures, the thickness of the insulation layer should be higher as well, and thus increase the overall system weight and volume. Nevertheless, as the walls have to be thicker (thus heavier) in the vacuum-insulation and MLI case, in order to feature a higher mechanical resistance to the pressure difference, this weight penalty is somehow the same in both cases.

Such possible insulating systems based on foams or MLI are visible on Figure 12, where the two designs studied by [VER-10] are exposed. Indeed, a combination of the three methods described previously can be imagined to develop the tank insulating system (the "MLI" design of [VER-10] uses for instance an MLI layer as well as a foam layer).

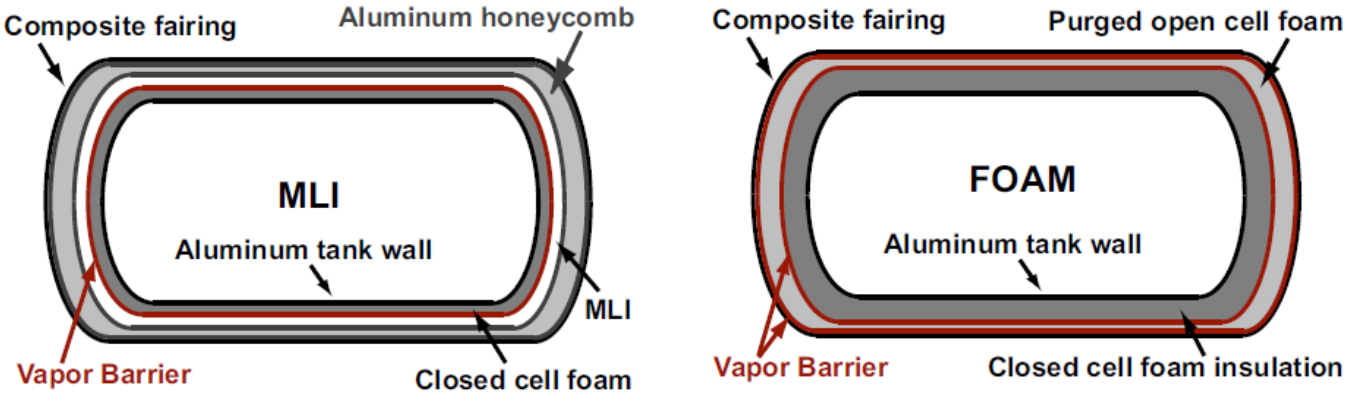

Figure 12 – Two possible insulating structures for LH_2 tanks (MLI and FOAM) investigated in [VER-10] for regional aircraft

Studies investigating on the design of future tanks for aircraft applications such as [VER-10] or [WIN-18], show that gravimetric index up to 71 wt. % ([VER-10]) and 64 – 70 wt. % ([WIN-18]) could be reached for regional aircraft (vs. 75 wt. % in the case of kerosene tanks, [WIN-18]). These high values should nevertheless be contextualized with respect to the amount of H_2 stored in these tanks (~ 1150 kg_{H2} in the [VER-10] study).

Indeed, **the weight of the tank is proportional to the wall surface** (the wall thickness depends on the insulating method and on the heat leak but not on the tank volume or surface), whereas **the weight of the embedded LH_2 is proportional to the tank volume**. Hence, **the higher the H_2 embedded mass is, the higher the gravimetric efficiency of the tank will be** (cf. equation (1)).

While these theoretical studies are concentrated on the design and potential use of LH_2 tanks for future aircrafts (without demonstration prototypes or experimental values available), a LH_2 storage system has already been embedded in a small UAV coupled with a LT-PEMFC ([STR-14]). Despite the small quantity of H_2 stored inside the tank (1.34 kg_{H2}), the

gravimetric efficiency of the storage system reached 23 wt. % and the H_2 volumetric capacity 0.036 kg_{H2}/L. The authors used there an MLI and vacuum insulation system between a double-wall structure (cf. Figure 13), as well as a heater and pressure relief valves (MPRV and SPRV for Mechanical and Solenoid Pressure Relief Valves on the figure) to manage the boil-off and the H_2 pressure inside the tank as well as the FC H_2 feed.

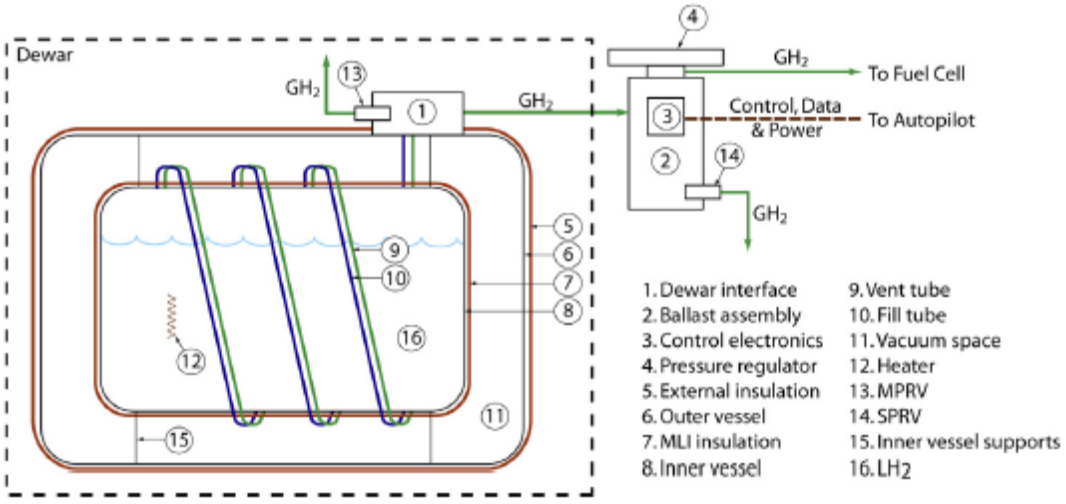

Figure 13 - LH_2 storage system (schematic) used in [STR-14] (Ion Tiger UAV)

One of the issue underlined by the authors ([STR-14]) is the H_2 loss due to LH_2 boil-off during the mission: even with a small heat leak, H_2 has to be vented regularly if it is not consumed by the FC. In [WIN-18], the authors underline that this issue could be somehow compensated by imposing an adequate power load to the FC: as the evaporated H_2 would be consumed continuously through the FC, the pressure rise inside the tank would be limited and thus the H_2 loss through venting as well.

The spatial field has already been using liquid hydrogen, for the famous NASA Apollo's missions for instance ([BOW-06]). Liquid H_2 tanks were there embedded together with alkaline fuel cells (employed as power and water producing units). For this application, spherical tanks containing up to ~ 42 kg_{H2} each and showing a gravimetric efficiency of ~ 30 wt. % and a H_2 volumetric capacity of ~ 0.051 kg_{H2}/L were used (tank weight and volume of 98 kg and 820 L – outside diameter of 1.16 m, [BOW-06]).

Cryogenic LH_2 tanks have also been considered in automotive applications as an alternative fuel for direct combustion, especially by BMW. The BMW Hydrogen 7 sedan who has reached the series development step ([MUL-07]), features for instance LH_2 tanks (with a vacuum + MLI insulation) containing ~ 8 kg_{H2} each. Such tank and LH_2 storage system is well described in [AMA-06], as well as the different procedures to fill the tank, to manage the H_2 boil-off and the H_2 pressure inside the tank, and to control the H_2 feed to the combustion engine (cf. Figure 14). According to [DIC-18], the LH_2 tanks used in the BMW series 7 cars reach gravimetric efficiencies around 14.2 wt. % and H_2 volumetric capacities of 0.042 kg_{H2}/L (51.5 kg and 200 L tanks with a venting pressure of 5 bara).

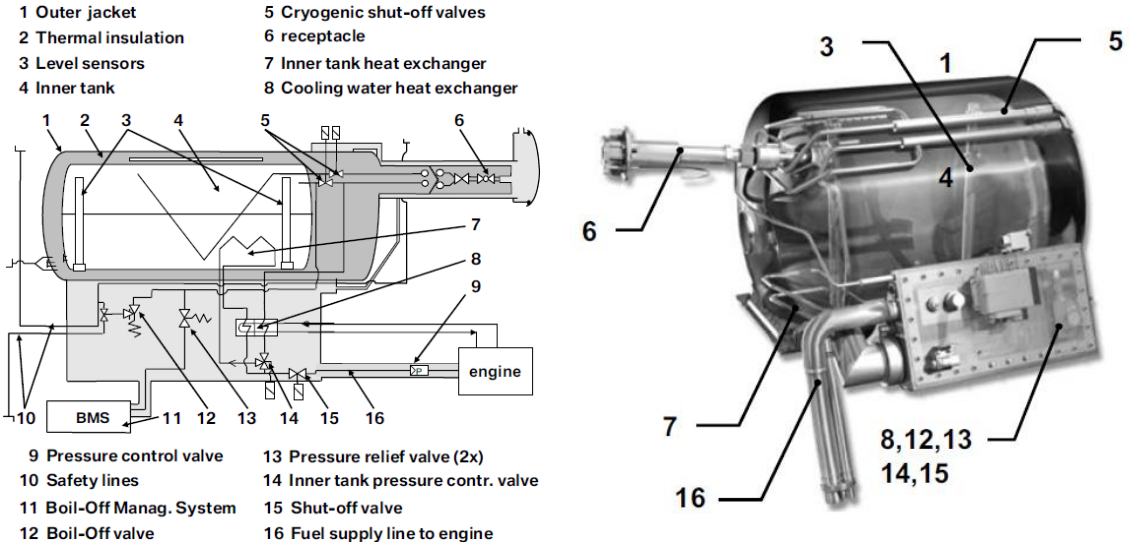

Figure 14 - BMW series 7 LH_2 storage system diagram and constitution ([AMA-06])

Air Liquide also developed various LH_2 tanks in collaboration with BMW ([MIC-06], [MIC-08]), particularly with a cylindrical LH_2 lightweight tank prototype reaching a gravimetric efficiency of 15 wt. % and a H_2 volumetric capacity of 0.04 kg_{H2}/L (the tank contains ~ 11.7 kg_{H2} with an empty weight of 66 kg and a volume of 291 L). Such value (15 wt. % gravimetric efficiency) is often referred to as an emblematic value for LH_2 storage systems when considering stored H_2 quantities in this order of magnitude (~ 10 kg_{H2}), for instance in [BEN-15].

Taking into account some of the LH_2 storages mentioned previously, a quick comparison with Figure 10 is made in Figure 15, where LH_2 storage systems performances are plotted in addition to the compressed H_2 composite storages.

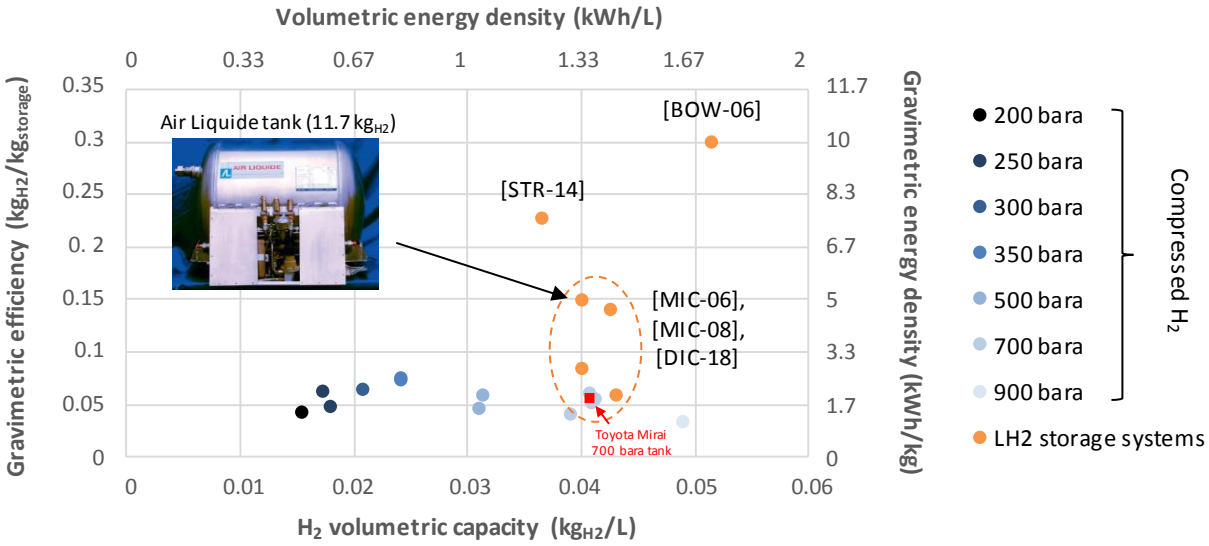

Figure 15 - Gravimetric efficiencies and H_2 volumetric capacity of different H_2 storages (derived from Figure 10)
Compressed H_2 storage data from [HEX-17]

Even if to be completely rigorous, other parameters like the H_2 mass stored in each tank should be precised when comparing such numbers, the graphic underlines the higher potential of LH_2 compared to compressed H_2 in terms of embedded mass and volume.

Regarding the energetic cost to liquefy H_2, [DIC-18] affirms that almost 40 % of the H_2 specific energy (LHV) is needed for the liquefaction process, which would be around 13.3 kWh/kg_{H2}. In [SIN-17], the authors mentioned a lower proportion of 30 – 33 % of the H_2 specific energy needed for the liquefaction (~ 10.5 kWh/kg_{H2}). Such values are much higher than the values mentioned previously (2.3.3.1) for the H_2 compression energetic cost (4.5 kWh/kg_{H2} for a compression at 700 bara); nevertheless, one work ([SAD-17]) claims that a much lower value of 4.41 kWh/kg_{H2} could be reached with a novel refrigeration process.

To sum up, very promising theoretical studies focused on future LH_2 storage systems for aeronautical applications, whether or not in order to be used as a fuel for direct combustion ([VER-10], [KHA-13]) or through a fuel cell ([WIN-18]), announce today possible gravimetric efficiencies in the order of 60 – 70 wt. % (in systems embedding more than 1000 kg_{H2}). Besides, such storage systems have already reached values up to 30 wt. % ([BOW-06]) in spatial applications. This value should however be considered with caution as the durability requirements are not the same in spatial and aeronautical applications (i.e. the LH_2 tanks were not designed to endure several duty cycles). On a specific application ([STR-14]), a value of 23 wt. % could be reached with a demonstration prototype storing a small H_2 quantity (1.34 kg_{H2}). In addition to these studies, the automotive industry has already been driving the development of LH_2 storage systems up to the serial production step and has consequently brought some important information about the actual level of performances of such storage systems ([MIC-06], [MIC-08], [AMA-06]). Considering these sources, values in the range of 14 – 15 wt. % for the gravimetric efficiency and 0.04 kg_{H2}/L for the H_2 volumetric capacity have already been demonstrated and can be considered as references for H_2 storage systems embedding H_2 masses around 10 kg_{H2}.

2.3.3.3. Metal Hydrides

Although compressed and liquid H_2 constitute today the most mature methods to embed hydrogen, storing H_2 through solid material can also be mentioned when scanning the different H_2 storage methods. Such approaches often use material like reversible metal hydrides that will have the ability to adsorb H_2 and to release it through chemisorption mechanisms driven by pressure and temperature cycles. These materials offer great performances in terms of H_2 volumetric capacity (0.05 kg_{H2}/L, [YOU-04]) but poor performances in terms of gravimetric efficiency (1.5 wt. %, [YOU-04]), behind the performances of compressed H_2 or Liquid H_2 storages. According to [BUS-16], values up to 7 wt. % and 0.045 kg_{H2}/L (and an availability of 90 % for the stored H_2) have been recently reached using sodium borohydrides material in an application with an UAV.

Despite the last value showing that there is room for improvement and interesting perspectives with this storage method with respect to the gravimetric efficiency and the H_2

volumetric capacity, some uncertainties remain concerning the ability of the material employed to withdraw large quantities of H_2 ([WIN-18]).

For this reason, and because to date state-of-the-art performances of such storages are behind compressed and liquid H_2 storages in terms of mass efficiency, metal hydrides and solid storages will not be considered further in this study.

2.4. Summary of the performances assessments made for the selected technologies

After having detailed some information about different technologies of battery, FC, and H_2 storages, considered in this study as potential parts of the auxiliary sources hybridizing the gas turbines in a future regional aircraft, this part will attempt to **summarize in a very synthetic way several values** representatives of their current and future (if evaluable) performances.

More specifically, typical values of specific energies, C_{rate} maximal limits and cycle life will be given on one hand for the battery technologies scanned in the 2.2.2 part (High power: LTO/TNO, High Energy: NMC, Very high energy: all solid state NMC and LiS); while on the other hand, estimated state of the art values of FC stacks specific power, auxiliaries specific weight / volume impact factor (for the LT PEMFC case) and H_2 storages gravimetric efficiencies and volumetric capacities (2.3.2 and 2.3.3 parts), will be assessed.

Two dates will be considered for the future performances evaluation: the years 2025 and 2035. Obviously, the collection of information as well as the lack of visibility on the development of several technological aspects (on the battery side and on the FC / H_2 storage side) is not necessarily providing clear answers for these projections, hence some blanks can appear in the forecast tables.

2.4.1. Battery: specific energies, C_{rate} capabilities and cyclability assessments

The first tables (Table 10 and Table 11) summarize the information scanned in the 2.2.2 part, respectively in terms of gravimetric and volumetric energy density for the selected technologies (LTO – high power, NMC – high energy and LiS – Very High Energy). In addition, two others technologies mentioned as well previously were added: the TNO on the high power side and the all solid state battery on the very-high-energy side.

Specific energy e_m (Wh/kg @ cell scale)	Today	2025	2035
High Power: LTO / TNO	~ 90 – 140 Wh/kg_{cell}	~ 160 – 180 Wh/kg_{cell}	~ 180 – 200 Wh/kg_{cell}
High Energy: NMC	~ 250 Wh/kg_{cell}	~ 350 Wh/kg_{cell}	~ 500 Wh/kg_{cell}
Very-high Energy: All Solid State (NMC)	~ 450 Wh/kg_{cell}	~ 550 Wh/kg_{cell}	~ 650 Wh/kg_{cell}
Very-high Energy: LiS	~ 500 Wh/kg_{cell}	~ 600 Wh/kg_{cell}	~ 650 Wh/kg_{cell}

Table 10 - Gravimetric energy density assessments (Wh/kg) for the selected technologies at the cell scale (cf. 2.2.2)

A few comments can be made regarding Table 10:

- LTO / TNO: the two technologies are put together because they feature a lot of common characteristics (nominal cell voltage, cyclability, C_{rate} performances…).
- NMC: the perspectives (2025 and 2035) are given considering the capabilities of cells using Si for the anode electrode.
- All solid state: we include with this term technologies using a Li metallic anode and a solid electrolyte (polymer) or a semi-solid electrolyte (ceramic + liquid electrolyte) with a high energy cathode (NMC).

Specific energy e_v (Wh/L @ cell scale)	Today	2025	2035
High Power: LTO / TNO	~ 180 – 350 Wh/L_{cell}	~ 320 – 450 Wh/L_{cell}	~ 360 – 500 Wh/L_{cell}
High Energy: NMC	~ 650 Wh/L_{cell}	~ 900 Wh/L_{cell}	~ 1250 Wh/L_{cell}
Very-high Energy: All Solid State (NMC)	~ 900 – 1000 Wh/L_{cell}	~ 1150 Wh/L_{cell}	~ 1300 Wh/L_{cell}
Very-high Energy: LiS	~ 300 Wh/L_{cell}	~ 600 Wh/L_{cell}	~ 650 Wh/L_{cell}

Table 11 - Volumetric energy density assessments (Wh/L) for the selected technologies at the cell scale (cf. 2.2.2)

Regarding the estimation of the volumetric energy density forecasts on Table 11, the following hypothesis was taken: if no specific information was available, a constant kg/L ratio was considered at the cell scale to evaluate the Wh/L_{cell} future projections. To jump from the cell to the system scale assessments of the gravimetric and volumetric energy densities, constant integrating factor parameters (f_m and f_v) are considered, as developed in the 2.2.3 section. Their values are estimated to be respectively $\boldsymbol{f_m = 2}$ **and** $\boldsymbol{f_v = 2.5}$.

The power capabilities of the selected technologies are appraised in Table 12 where the C_{rate} performances are put for the charge and discharge options. Indeed, the values specified here refer to the C_{rate} limits given by some manufacturers (cf. 2.2.2) for the maximum continuous charge and/or discharge speeds. The information displayed here does not specify however the peak power capabilities of each technology (which will be higher than the maximum continuous charge/discharge power).

C_{rate} capabilities (charge / discharge)	Today	2025	2035
High Power: LTO / TNO	3 – 10C / 3 – 10C	-	-
High Energy: NMC	0.5C / 2C	-	-
Very-high Energy: All Solid State (NMC)	0.2C / 2C	-	-
Very-high Energy: LiS	0.2C / 1C	-	-

Table 12 - C_{rate} capability assessments for the selected technologies (cf. 2.2.2)

Additionally, the charge / discharge speed will have an impact on the available energy for a given battery mass, and therefore the expected energy/power will somehow be different depending on the charge/discharge characteristics of each technology. Let's assume for

instance that 1 kWh of battery is embedded and that this battery maximal continuous discharge speed is about 2C: the expected 1 kWh / 2 kW capabilities of the embedded battery will quite probably be lower, due to the battery discharge speed (through the effect of the electrochemical losses and/or Peukert effect on the battery capacity). This aspect will be further developed in the next part (cf. 3.3.1), through a modeling approach based on the Tremblay-Dessaint equations ([TRE-09]).

Information collected about the typical cycling life of the different battery technologies is reported in Table 13. The cycling numbers specified here refer to the charge/discharge cycles (if not specified: up to 80 % DoD) that can be reached until a 20 % capacity loss.

Cyclability (charge / discharge cycles)	Today	2025	2035
High Power: LTO / TNO	Up to 15000 cycles (100 % DoD)	Up to 20000 cycles (100 % DoD)	-
High Energy: NMC	> 300 cycles	-	-
Very-high Energy: All Solid State (NMC)	200 cycles	-	-
Very-high Energy: LiS	100 cycles	500 – 1000 cycles	-

Table 13 - Cyclability assessments for the selected technologies (cf. 2.2.2)

The charge / discharge speeds associated to this cycling life are often at nominal conditions (cf. Appendix A for instance), however in the case of LTO/TNO cells the charge/discharge speeds were much higher during the cycling tests (15000 cycles at 3C/3C for the LTO for instance, [TOS-17]).

Also, even if this aspect is not much covered in this work, one should as well take into account the thermal performances of the selected technologies as well as the dependence of the other performances indicators to the working temperature (cell specific energy / C_{rate} capabilities / cyclability).

2.4.2. Fuel Cell stacks and systems specific power / H_2 storage performances

Looking the different technologies of Fuel Cell stacks and systems considered here, Table 14 proposes a summary of the different datasheets and articles reviewed in the 2.3.2 part. The FC stack specific power values refer to the ratio between the FC stack output power and its mass / volume, whereas the FC system specific power values refer to the ratio between the FC system net output power (considering the FC stack auxiliaries parasitic power consumption) and the total system mass / volume (the denomination “system” referring here to the power conversion part, i.e. without considering the energy storage brick).

Indeed, as already precised previously, it is quite delicate to assess current and future level of performances of the HT PEMFC and SOFC technologies at the stack and at the system level, due to their lack of maturity. For the LT PEMFC, more information are available at the stack and at the system scale. Although a certain uncertainty remains concerning the current LT

PEMFC system power performances (as all the auxiliary components are not compulsorily included in all the datasheets or articles reviewed, cf. Table 8), several values can be estimated around 0.6 and 0.7 kW/kg$_{system}$ by looking to the few communications bringing information at the system scale including all the Balance of Plants components ([IE-15], [POG-18]).

FC stack and system specific power densities p_m / p_v (kW/kg and kW/L)	Today	2025	2035
LT PEMFC	~ 2 – 3 kW/kg$_{stack}$ ~ 0.6 – 0.7 kW/kg$_{system}$	~ 4 kW/kg$_{stack}$ ~ 1 kW/kg$_{system}$	> 5 kW/kg$_{stack}$ > 1.1 kW/kg$_{system}$
	~ 3 – 3.5 kW/L$_{stack}$ ~ 0.3 – 0.6 kW/L$_{system}$	~ 5 kW/L$_{stack}$ ~ 0.8 kW/L$_{system}$	> 6 kW/L$_{stack}$ > 0.9 kW/L$_{system}$
HT PEMFC	~ 0.4 – 0.8 kW/kg$_{stack}$	~ 1 kW/kg$_{stack}$	-
SOFC	~ 0.33 kW/kg$_{stack}$	-	-

Table 14 - Fuel Cell stack / system (gravimetric and volumetric) specific power densities (cf. 2.3.2.1 & 2.3.2.3)

The projections values (~ 1 kW/kg$_{system}$ for 2025) are estimated not only by updating the estimations of the stack specific powers, but also the auxiliary specific weight / volume impact (presented Table 15), and by considering improvements of the FC stack and system efficiencies at nominal power: from 0.5 (today) to 0.55 (2025 and 2035) for the FC stack efficiency η_{FC}^{stack} and from 0.42 to 0.5 for the FC system efficiency η_{FC}^{system}.

The auxiliaries specific weight and volume impact factor (p_m^{aux} and p_v^{aux} respectively) are estimated according to the calculations made in 2.3.2.2 and displayed in Table 15. It should be emphasized here that these rough estimations are made for LT PEMFC systems and that the p_m^{aux} and p_v^{aux} values should vary when considering HT PEMFC or SOFC systems (and probably increase, i.e. the auxiliaries mass should decrease). Also, it is precised here again that these values represent respectively the ratio between the FC stack output power (P$_{gross}$) and the auxiliaries mass and volume (cf. equation (6)).

Auxiliary specific weight / volume impact parameter (p_m^{aux} / p_v^{aux})	Today	2025	2035
LT PEMFC	1.15 kW$_{gross}$/kg 0.94 kW$_{gross}$/L	1.5 kW$_{gross}$/kg 1.2 kW$_{gross}$/L	1.75 kW$_{gross}$/kg 1.4 kW$_{gross}$/L

Table 15 - Auxiliaries specific weight / volume impact parameter (cf. 2.3.2.2)

In order to estimate some projections for 2025 and 2035, improvements of respectively 30 % and 50 % were assessed on the cooling system mass and volume as well as on the other auxiliary components (compressor and H_2 recirculator masses and volumes).

In addition to the previous tables focused on the power conversion part, Table 16 summarizes the current performances and forecasts for the H_2 storage brick. In order to give some orders

of magnitude in terms of specific energies, two values are added (each associated to the different storage methods considered): a "gross" value based on the gravimetric efficiency of the storage method and on the H_2 LHV ($kWh_{gross}/kg_{storage}$), and a "net" value taking additionally into account the conversion efficiency of the FC system block and representing thus a "useable" specific energy ($kWh_{net}/kg_{storage}$).

H_2 storage gravimetric efficiencies (-) and specific energy (Wh/kg based on H_2 LHV)	Today	2025	2035
Compressed H_2 (700 and 350 bara)	~ 5 – 7.5 wt. % ~ 1.67 – 2.5 kWh/kg (0.7 – 1 kWh/kg*)	~ 10 wt. % ~ 3.3 kWh/kg (1.67 kWh/kg**)	> 10 wt. % > 3.3 kWh/kg (> 1.67 kWh/kg**)
Liquid H_2 (~ 20 K)	~ 15 wt. % ~ 5 kWh/kg (2.1 kWh/kg*)	~ 20 wt. % ~ 6.6 kWh/kg (3.3 kWh/kg**)	> 20 wt. % > 6.6 kWh/kg (> 3.3 kWh/kg**)
Solid (metal hydrides)	~ 2 – 3 wt. % ~ 0.67 – 1 kWh/kg (0.28 – 0.42 kWh/kg*)	~ 7 wt. % ~ 2.3 kWh/kg (1.15 kWh/kg**)	> 7 wt. % > 2.3 kWh/kg > 1.15 kWh/kg**

* useful energy assuming a FC system efficiency of 0.42 ; ** useful energy assuming a FC system efficiency of 0.5

Table 16 - H_2 storage gravimetric efficiencies (wt. %) and specific energies (kWh/kg) – cf. 2.3.3 & Figure 15

Regarding the H_2 volumetric capacity ($kg_{H2}/L_{storage}$), the values of compressed H_2 composite tanks are already closed to the theoretical value of the H_2 densities under such pressures, i.e. 0.024 kg_{H2}/L (~ 0.8 kWh_{gross}/L and 0.3 – 0.4 kWh_{net}/L considering a FC system efficiency η_{FC}^{system} around 0.4 – 0.5) at 350 bara and 0.041 kg_{H2}/L (~ 1.36 kWh_{gross}/L and 0.6 kWh_{net}/L considering a FC system efficiency η_{FC}^{system} around 0.4 – 0.5) at 700 bara. These numbers cannot obviously be improved in the next decades for physical reasons (density of compressed H_2). For LH_2 storages, values up to 0.04 kg_{H2}/L (~ 1.33 kWh_{gross}/L and 0.6 kWh_{net}/L considering a FC system efficiency η_{FC}^{system} around 0.4 – 0.5) are reached today for H_2 quantities around 10 kg with automotive tanks (cf. Figure 15), while the theoretical limit is around 0.071 kg_{H2}/L. In the same way as for the gravimetric efficiencies, these values are of course highly dependent on the stored H_2 quantity: the more H_2 is carried, the higher the volumetric capacity is. In terms of perspectives, if we assume a constant H_2 quantity, the only way to improve the H_2 volumetric capacity is to reduce the insulation thickness which seem however quite challenging. Also, it should be taken into account that due to venting pressures superiors to 1 bara, the actual H_2 density inside the LH_2 tank will be lower than 0.071 kg_{H2}/L ([WIN-18]), decreasing as well the theoretical target limit.

High H_2 volumetric capacities are reached today with the solid storages based on metal hydrides (cf. 2.3.3.3) with values up to 0.045 – 0.05 kg_{H2}/L (~ 1.66 kWh_{gross}/L and 0.7 – 0.8 kWh_{net}/L considering a FC system efficiency η_{FC}^{system} around 0.4 – 0.5). Although such technologies could be the most promising in terms of H_2 volumetric capacity, it is quite

delicate to estimate some future projections due to their lack of maturity. In addition, their poor gravimetric efficiency is to date a showstopper for weight sensitive applications such as aeronautical ones.

2.4.3. First comparison at the system scale between FC and batteries on a particular case

Anticipating a little bit on part 3, this section will try to make a **short first comparison at the system scale between the different battery technologies and a LT PEMFC + LH_2 association**, in terms of specific energy and specific power (Table 17 & Table 18).

As there are no intrinsic values of specific energy or specific power linked with any association of one FC technology with one H_2 storage method (both values depend on the specific mass of each part of the system – the power conversion part and the energy storage part – which in returns depends on the energy and power requirements of the mission), a particular case is considered here. More specifically, a light hybridization scenario (cf. 3.1) is taken as reference with a maximal power requirement of 280 kW and a total energy requirement of 157 kWh.

For the sake of simplicity, only one {FC + H_2 storage} association is considered: the one presenting the best current performances respectively for the FC system power conversion part (LT PEMFC) and for the H_2 storage gravimetric efficiency (LH_2 tank(s)).

Specific energy at the system scale (Wh/kg)	Today	2025	2035
High Power: LTO/TNO	~ 70 Wh/kg	~ 90 Wh/kg	~ 100 Wh/kg
High Energy: NMC	~ 150 Wh/kg	~ 225 Wh/kg	~ 250 Wh/kg
Very-High Energy: All solid state (NMC)	~ 225 Wh/kg	~ 275 Wh/kg	~ 325 Wh/kg
Very-High Energy: LiS	~ 250 Wh/kg	~ 300 Wh/kg	~ 325 Wh/kg
LT PEMFC + LH_2*	**~ 300 Wh/kg**	**~ 480 Wh/kg**	**~ 550 Wh/kg**

* Study case: assuming 280 kW and 157 kWh needs to estimate the LT PEMFC + LH_2 system case

Table 17 - Evaluation of specific energies at the system scale between batteries and a {LT PEMFC + LH_2 storage} potential association (cf. Table 10, Table 14, Table 15 & Table 16)

In order to evaluate the values presented Table 17 & Table 18, several hypotheses are assumed:

- On the battery side, the specific energies at the system scale are assessed by dividing the specific energies at the cell scale (presented Table 10) by the integrating factor f_m ($f_m = 2$). Regarding the specific powers at the system scale (Table 18), at first approximation their values are assessed by multiplying the specific energies at the system scale with the maximal C_{rate} capacities associated to the battery technologies (in **continuous discharge** mode here). The actual values should nevertheless be lower due to the different losses presents during the energy conversion, lowering both the specific energies and specific powers values.

- On the FC side, based on Table 14, Table 15 & Table 16, the FC system mass and H_2 storage mass are first assessed with respect to the mission requirements (280 kW and 157 kWh), and in a second time the specific energy and power at the system scale can be evaluated knowing the power and energy capabilities of the system with respect to its total mass.

Specific power at the system scale (kW/kg)	Today	2025	2035
High Power: LTO/TNO	~ 0.7 kW/kg	~ 0.9 kW/kg	~ 1 kW/kg
High Energy: NMC	~ 0.25 kW/kg	~ 0.35 kW/kg	~ 0.5 kW/kg
Very-High Energy: All solid state (NMC)	~ 0.45 kW/kg	~ 0.55 kW/kg	~ 0.65 kW/kg
Very-High Energy: LiS	~ 0.25 kW/kg	~ 0.3 kW/kg	~ 0.32 kW/kg
LT PEMFC + LH_2*	**~ 0.53 kW/kg**	**~ 0.85 kW/kg**	**~ 1 kW/kg**

* Study case: assuming 280 kW and 157 kWh needs to estimate the LT PEMFC + LH_2 system case

Table 18 – Evaluation of specific powers at the system scale between batteries and a {LT PEMFC + LH_2 storage} potential association (cf. Table 10, Table 12, Table 14, Table 15 & Table 16)

Even if these tables are focused on a particular case and based on roughly estimated numbers, they allow a first comparison between the battery technologies and FC capacities. This first appraisal shows better results on the FC side for missions showing such energy and power requirements (regarding the current and future performances) with all the hypotheses taken previously.

In order to go deeper into the evaluation of the hybrid auxiliary source mass, as well as to investigate its behavior in terms of aspects such as efficiency, heat release, impact of the C_{rate} on the available energy for the battery case for instance, the next part is going to present several modeling developments on the battery and FC sides.

3. Mass estimations based on a simplified light hybridization mission and modeling developments for the Battery / Fuel Cell block

While part 2 proposed a review of different battery, FC system and H_2 storages, considered as potential candidates for the auxiliary source in a hybrid-electrical aircraft, this part is going to investigate more concretely on the auxiliary source modeling and on its mass evaluation accordingly to the objectives presented during the introduction.

In order to consider a specific case, an emblematic power mission is going to be firstly detailed (corresponding to the evaluation made in 2.4.3). Modeling developments will be presented further to assess some masses corresponding to the power missions presented, and to give some insights into the auxiliary source behavior during the mission (regarding parameters such as efficiency, heat release…). The modeling developments will be first introduced with a simplified approach giving a "first level" evaluation of the auxiliary source mass, while a more refined approach ("second level" estimation of the masses) will be given afterwards.

3.1. Power profile mission(s) taken as reference(s)

As already briefly specified in the 2.4.3 part, the reference mission is corresponding to a "light hybridization" scenario case: the auxiliary source is exclusively used during the taxi phases (taxi-in and taxi-out) and during the descent step, while the gas turbines handle the rest of the mission. Assuming that the non-propulsive loads can be estimated to a constant 140 kW, the entire power mission corresponding to a light hybridization scenario can be assessed and is presented Figure 16.

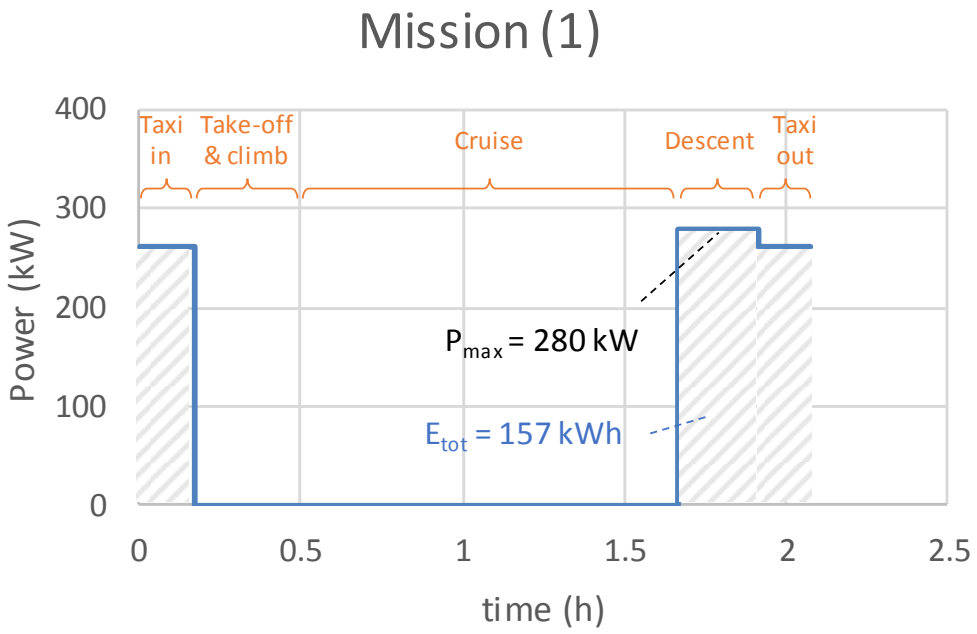

Figure 16 - Auxiliary source power mission ("light hybridization" scenario) - Mission (1): taxi in and out and descent phases (considering constant non-propulsive loads of 140 kW)

Such mission – referred to as Mission (1) – would require from the auxiliary source an amount of energy of ~ 157 kWh with a max power of 280 kW. As batteries are considered as a potential auxiliary source in this study, an alternative version of this light hybridization scenario is also considered with a recharge phase during the cruise period. This alternative version of the light hybridization scenario only concerning batteries is presented in Figure 17. In this particular case, the amount of energy provided by the auxiliary source (i.e. the battery here), not originate from the recharge (energy from the kerosene combustion), would decrease from 157 to 113 kWh.

Obviously, the two missions presented here are not necessarily representing an optimal power sharing strategy regarding the overall kerosene consumption or any other global design parameters, but they constitute fixed examples to illustrate the modeling developments purpose. In a complementary step, the modeling tools presented further are meant to be used as analytic tools in order to investigate the sensitivity of some global systemic parameters (such as the overall kerosene consumption during the mission) to the power sharing strategy and the auxiliary source power mission. The reader is referred to the Matthieu Pettes-Duller PhD work (WP6), for deeper developments on these aspects.

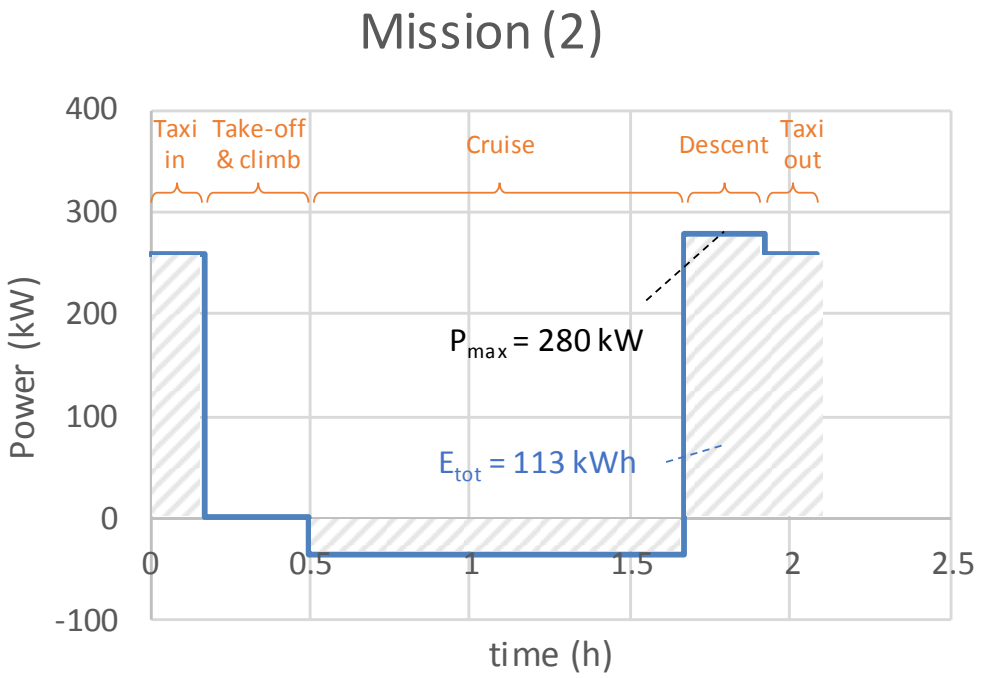

Figure 17 - Auxiliary source power mission (battery case only) - Mission (2): taxi in and out and descent phases (considering constant non-propulsive loads of 140 kW) with a recharge during the cruise

Note: even if temporal dynamic aspects are not examined in this work, one should however consider beside the main energy source the presence of a buffer device – such as a supercapacitor pack and/or a high power type battery (LTO for instance) – in order to handle the load dynamic variations. If we take for instance the FC system case, a slow dynamic response of the air compressor to the power steps Figure 16 could limit the dynamic capacities of the entire FC system, and the presence of a buffer device would be therefore necessary.

3.2. First level mass estimations

In order to give a rough estimation of the auxiliary source mass depending on the power mission requirements and on the different technologies selected, two equations (eq. (12) and (13)) are used respectively for the battery block and for the FC system & H_2 storage block. The expressions are presented here only for the mass evaluation of the auxiliary source in order to keep the document to a reasonable size, however the parameters used (f_m, e_m, η_m, p_m^{FC}, p_m^{aux}) can be as well transposed in their volumetric form (f_v, e_v, η_v, p_v^{FC}, p_v^{aux}) to evaluate the auxiliary source volume.

$$m_{Battery} = max\left(\frac{E_{tot}}{e_m} * f_m \,; \frac{P_{max}}{(C_{rate}^{max}) * e_m} * f_m\right) \qquad (12)$$

$$m_{\{H_2\ storage\ /\ FC\ system\}} = \frac{E_{tot}}{\left(\eta_m * LHV * \eta_{FC}^{system}\right)} + \left(\frac{P_{max}}{p_m^{FC}} + \frac{P_{max}}{p_m^{aux}}\right) * \frac{\eta_{FC}^{stack}}{\eta_{FC}^{system}} \qquad (13)$$

Some parameters used in these equations have already been introduced previously (cf. equations (1) to (11) and 2.1), however for the sake of clarity they are listed again below:

- E_{tot} (kWh) and P_{max} (kW) correspond respectively to the auxiliary source energy requirement and maximal power requirement (in absolute value for the battery charge case) for the given power mission.
- e_m (expressed here in kWh/kg) is the battery gravimetric energy density at the cell scale.
- f_m (kg_{system}/kg_{cell}) is the battery weight integrating factor accounting for the mass of the battery packaging, BMS and cooling system.
- C_{rate}^{max} (h^{-1}) is the battery maximal continuous charge/discharge (corresponding to the P_{max} sign) rate.
- η_m is the H_2 storage gravimetric efficiency ($kg_{H2}/kg_{storage}$) and LHV is the Lower Heating Value of H_2 (33.3 kWh/kg_{H2}).
- η_{FC}^{stack} and η_{FC}^{system} (-) are respectively the FC stack and FC system power conversion efficiencies at maximal power (equations (9) and (10)).
- p_m^{FC} (kW/kg) is the gravimetric power density of the FC stack.
- p_m^{aux} (kW_{FC}/kg_{aux}) is the FC auxiliaries specific weight impact (with respect to the FC gross power).

These two equations ((12) and (13)) represent basic sizing rules based on the bibliographic review made in part 2.

For the battery mass expression (equation (12)), two sizings are compared:

- An "energy" one ($\frac{E_{tot}}{e_m} * f_m$): the energy requirement of the mission (maximal energy charged/discharged by the battery during the mission) is the sizing criterion.
- A "power" one ($\frac{P_{max}}{(C_{rate}^{max})*e_m} * f_m$): the maximal power (in charge and discharge mode) and the corresponding maximal continuous charge/discharge rate are the sizing criteria: the battery is sized in order not to exceed the C_{rate}^{max} limit in charge or discharge mode.

The maximum value between both evaluations is finally the mass estimation of the battery block. Obviously, several simplifying hypotheses are underlaid in this expression: no battery losses are considered for instance which not only consists in assuming a 100 % battery conversion efficiency but also in assuming that the C_{rate} has no impact on the energy and power capacities of the battery. Also, no margin are taken regarding the SOC limits during the mission and the impact of the packaging and cooling system mass is integrated using a simple multiplying factor f_m.

For the {FC system + H_2 storage} mass equation (eq. (13)), the H_2 storage part is evaluated with respect to the mission energy requirement E_{tot}, the FC system conversion efficiency and the H_2 storage gravimetric efficiency, while the FC system part depends not only on the stack gravimetric power density and the auxiliaries weight impact factor, but also on the power

requirement at the stack scale (hence on the mission maximal power requirement and the efficiencies at the stack and at the system scale). Obviously, as for the battery mass equation, a few hypotheses are underlaid in equation (13): the H_2 storage gravimetric efficiency is considered constant and independent on the H_2 mass stored for instance, and fixed efficiencies at the system and stack scale are assumed. Furthermore, as already developed previously (2.3.2.2), a single parameter (p_m^{aux}) is considered for the auxiliary mass evaluation. Furthermore, for the whole FC system part it is assumed that the design point is the stack maximum power point (the stack maximum power capacity is equal to its maximal power requirement during the mission), while one could imagine moving this design point to impact the overall system mass and maybe minimize it, as it will be developed in 3.3.2.

Using these two equations and the values summarized in 2.4 (Table 10, Table 12 for the battery equation, and Table 14, Table 15, Table 16 for the FC one), it is possible to make a first assessment for the auxiliary source mass depending on the technology considered.

Regarding the FC technologies, only the LT PEMFC results associated with two H_2 storage technologies, compressed H_2 (CH_2) at 700 bara and LH_2, are shown. Results of these masses evaluations are presented in Figure 18 for the two missions (respectively in blue and red for Mission (1) and (2)). It is worth noting that the results presented for Mission (1) in this figure are the ones corresponding to the values of gravimetric energies and powers densities displayed in Table 17 and Table 18.

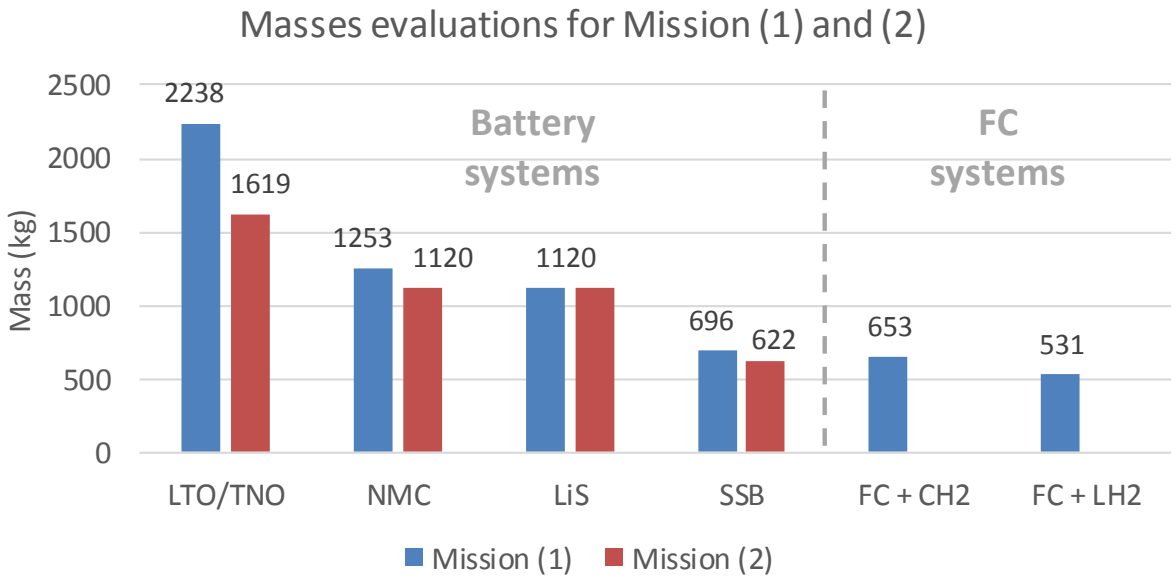

Figure 18 - Masses evaluations of the Battery / {FC + H_2 storage} systems for the missions presented Figure 16 and Figure 17 (today values)

A global overview of these results shows at first sight (and considering all the simplifying hypotheses detailed previously) a superiority of the FC systems compared to the battery ones in terms of mass for these power missions. A minimum of around 531 kg is especially reached with the {FC + LH_2} combination for Mission (1). On the battery side, these results obviously

confirm that the more energetic technologies – i.e. LiS and SSB – have better results than NMC and LTO/TNO for the energy/power requirements of these missions (SSB mass is lower than LiS mass because SSB C_{rate}^{max} value – 2C – is higher than LiS C_{rate}^{max} value – 1C). Besides these estimations, one should however consider the cyclability aspects already mentioned in part 2.2.2. Indeed, there is a clear trend showing that the most energetic technologies are often the technologies with the worst cyclability (Table 13): **it should be highlighted here that the best solutions regarding the mass Figure 18, are at the same time the ones showing the poorest cyclability**.

Obviously the mass results can widely vary depending on the two mission parameters in equations (12) and (13) – E_{tot} and P_{max}: the P_{max}/E_{tot} ratio, which could be considered as a mean equivalent C_{rate}, is actually a key parameter to understand what technology can be the best appropriated for a given mission profile in terms of mass. In order to illustrate this point, a case study assuming an energy requirement E_{tot} of 1 kWh and varying values of the P_{max}/E_{tot} ratio can be considered: Figure 19 show in particular the evolution of the different masses with the P_{max}/E_{tot} ratio and according to equations (12) and (13).

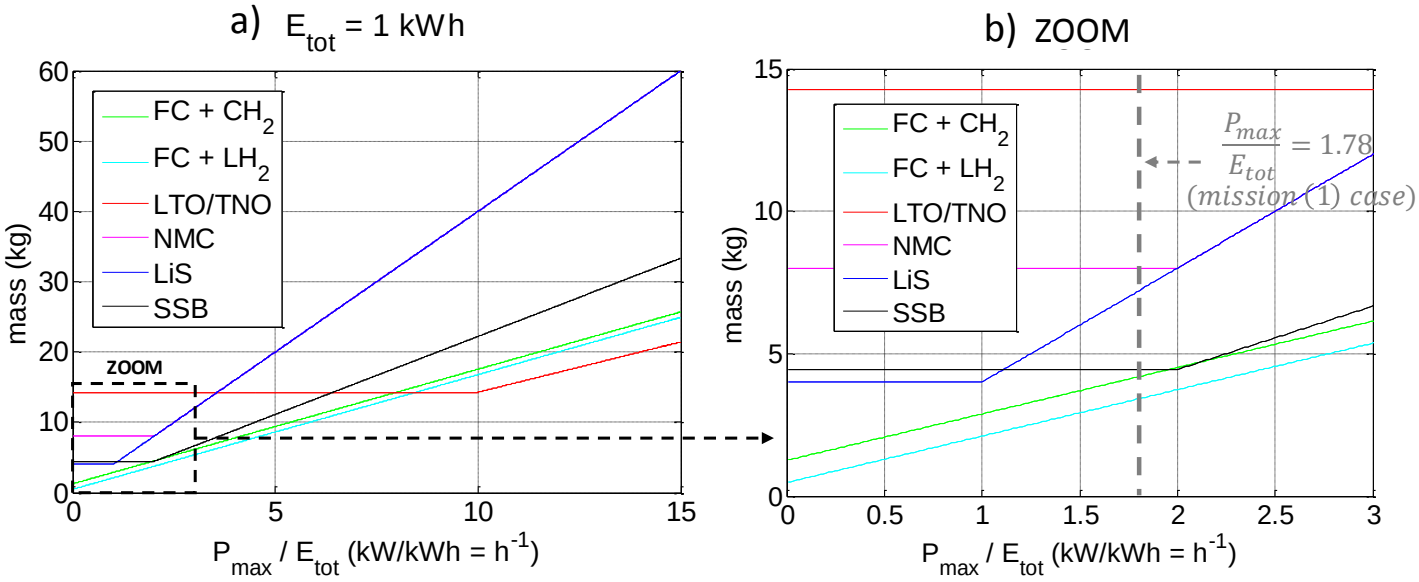

Figure 19 - Evolution of the battery / FC system masses (eq. (12) and (13)) with the P_{max}/E_{tot} ratio considering an energy requirement E_{tot} = 1 kWh / zoom for low values of P_{max}/E_{tot} in b)

The juxtaposition of the masses variations for each technology, depending on the P_{max}/E_{tot} ratio, highlights in Figure 19 that the minimum mass is not always reached by the same technology: in some areas ($P_{max}/E_{tot} > 8.5$), technologies such as LTO/TNO are lighter than the FC options, while for lower P_{max}/E_{tot} values (zoom Figure 19 – b)), FC systems and SSB technologies are the lightest options.

The graphics in Figure 19 highlights also for each battery technology a break in the curve when $P_{max}/E_{tot} > C_{rate}^{max}$, i.e. where the "power" sizing $\frac{P_{max}}{(C_{rate}^{max})*e_m} * f_m$ becomes superior to the "energy" one $\frac{E_{tot}}{e_m} * f_m$ (cf. equation (12)).

In order to provide more insights into the auxiliary source behavior during the mission, as well as to give a more refined estimation of its mass, several aspects related to the auxiliary source modeling are investigated in the following paragraphs. Knowing the simplifying hypotheses associated to the first level mass model presented in equations (12) and (13), some aspects are especially scrutinized for these modeling developments:

- On the battery side: a loss model integrating the dependence between parameters such as the SOC, the C_{rate}, the discharge / charge power or the conversion efficiencies seems compulsory in order to understand the battery electrical and thermal behavior (in a global way), as well as the actual sizing criterion (SOC, max discharge/charge current, or voltage limits).
- On the FC side: the understanding of the dependencies between the FC stack and system efficiencies and the stack size as well as the couplings between the auxiliary systems and the FC stack seem to be a compulsory step in order to improve the understanding of such systems during the mission.

3.3. Second level mass estimations and modeling developments

The battery modeling developments will be exposed together with the battery block sizing method in a first time, while the FC system and H_2 storage modeling and sizing method will be detailed after.

3.3.1. Battery behavior modeling

In order to describe, for each battery technology, the evolution of the battery conversion losses with parameters such as the State of Charge (SOC) or the C_{rate}, the Tremblay-Dessaint based equations are used ([TRE-09]). The equation (14) developed in [TRE-09] (without including dynamic effects here), express in the discharge mode the battery voltage (V_{bat}) dependence to the battery discharged capacity (it in Ah) and discharge current (i in A) with 6 parameters: E0 (V) the nominal voltage, A (V) and B ($(Ah)^{-1}$) respectively the exponential zone amplitude and time constant, K_{pol} (V/Ah) and K_{res} (Ω) the polarization constant and resistance and R the internal resistance (Ω). Q represents here the battery capacity (Ah).

$$V_{bat} = \boldsymbol{E0} + \boldsymbol{A} * e^{-\boldsymbol{B}*it} - \boldsymbol{K_{pol}} * it * \frac{Q}{Q - it} - \boldsymbol{R} * i - \boldsymbol{K_{res}} * i * \frac{Q}{Q - it} \qquad (14)$$

In order to associate these six parameters (E0, A, B, K_{pol}, K_{res} and R) to each battery technology introduced previously, emblematic cells are chosen for each technology: Toshiba cells (20 Ah SCiB cell and Toshiba R&D cell, [TAK-18]) for LTO and TNO, Panasonic cell (reference UR18650ZTA, [PAN-18]) for NMC, Oxis Energy pouch cell (POA0217, Appendix B) for LiS and Solid Energy ("Hermès" cell, Appendix A) for the SSB. For each of the technologies considered, the different sets of parameters are identified using available discharge curves characteristics of the reference cells, and through an optimization step minimizing the sum of the squared errors between the model and the measures. Figure 20

illustrates the modeling results for two technologies (TNO and NMC), after this identification step and the fitting accuracies (mean error < 2 %). The Tremblay-Dessaint equation is able to model quite faithfully all the discharge/charge behavior for the technologies selected, except for the LiS one, where the discharge/charge patterns are drastically different compared to the other technologies.

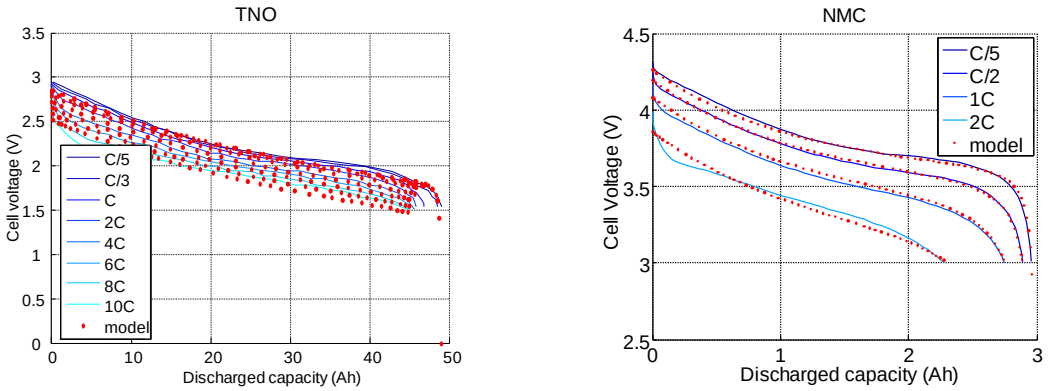

Figure 20 - Examples of modeling results (mean error < 2 %) with the Tremblay-Dessaint equation for two of the battery technologies considered (TNO and NMC)

Thanks to the parameters identification, the battery behavior during any power mission can be modeled and hence, a battery sizing can be evaluated. More precisely, a recursive algorithm is developed in order to find the minimal necessary cell number / mass able to fulfill a certain set of constraints: ***voltage constraints*** *(the cells should stay in a certain voltage working range),* $\boldsymbol{C_{rate}}$ ***constraints*** *(the cells should not be discharged/charged faster than certain speeds, cf. Table 12) and* ***SOC constraints*** *(some technologies – NMC, SSB, LiS – cannot be fully discharged and a margin – usually 20 % – should be kept). A first sizing step (oversizing the battery on purpose) initialize the sizing loop, then the number of cells is decreased step by step, and the minimal necessary cell number is identified to the last cell number respecting all the sizing constraints. Knowing the cell number, the cell mass and the system mass can be identified (by multiplying the cell mass with the integrating factor* f_m*).*

The sizing results are presented Figure 21 for the LTO, TNO, NMC and SSB (for the LiS case, no results are displayed as the modelling approach was not adapted to the LiS behavior):

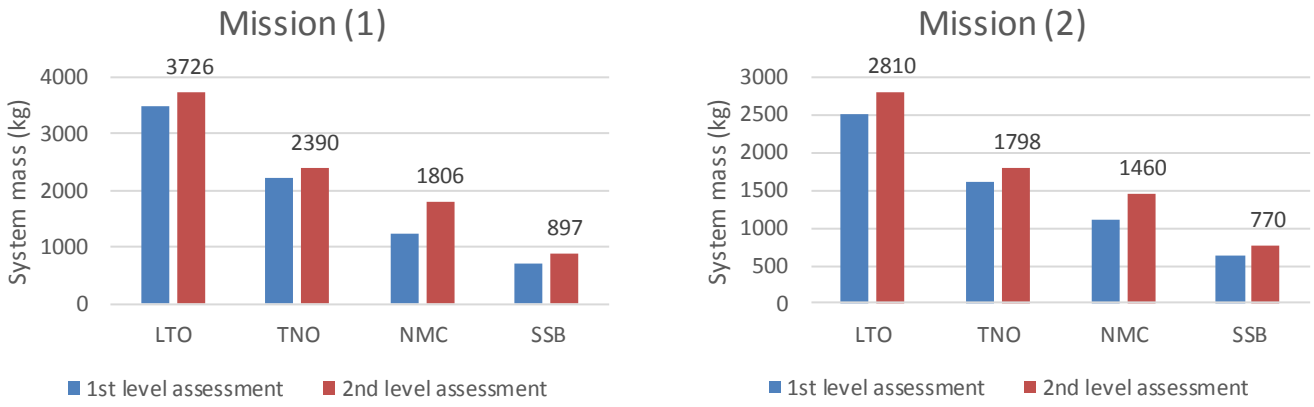

Figure 21 - Sizing results (in red) compared to the 1st assessment estimation (in blue)

In addition to the numerical simulations performed in order to assess the battery system masses, graphical tools in the Energy/Power plane are used to characterize each technology behavior during the missions. Thanks to the Tremblay-Dessaint equation (eq. (14)), iso-power charge and discharge characteristics are simulated and plotted in the Energy/power plane, considering the constraints detailed previously (voltage, C_{rate}^{max}, SOC), for each technology.

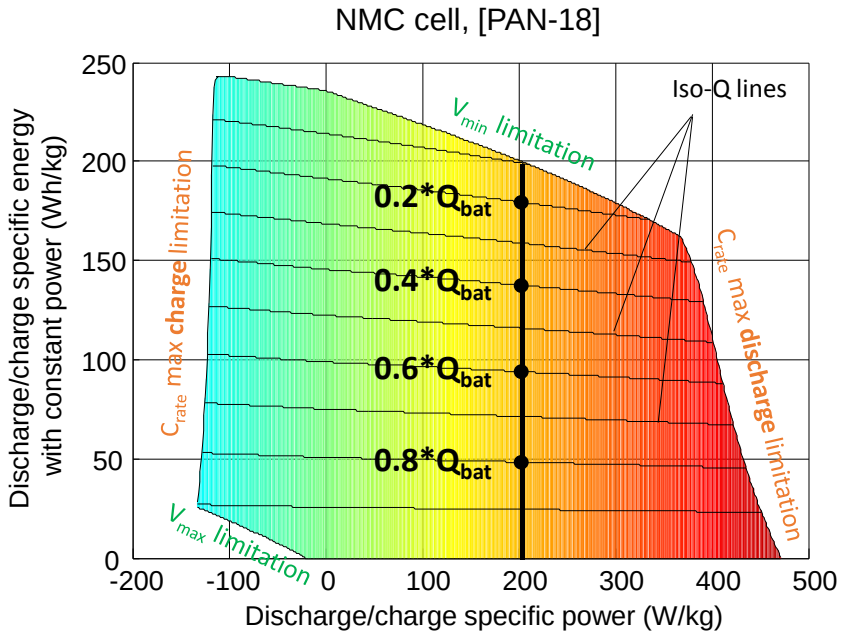

Figure 22 - NMC Panasonic cell ([PAN-18]) Energy/Power plot at constant discharge/charge powers

In Figure 22, an Energy/power plot for constant discharge/charge powers is shown for the NMC reference cell ([PAN-18]); values are normalized with respect to the cell mass in order to read directly the specific power and energy. In this plot, constant discharge/charge trajectories correspond to vertical lines, as highlighted in black for the 200 W/kg constant discharge from a fully charged state (discharged specific energy is equal to zero), to a maximum discharged specific energy of 200 Wh/kg for this discharge specific power (the minimum voltage constraint is in this example the dominant constraint if we don't consider the traditional SOC minimum margin of 20 %). This kind of plot illustrate in a graphic way how the available energy will vary with the charge/discharge power and the battery C_{rate}. Obviously, different plot shapes appear according to the battery technology. Also, as the available discharge specific energies depend on the discharge specific power, iso-Q (as well iso-SOC) lines (in black) are not horizontal lines in this plot: depending on the discharge power, the amount of energy that is delivered for a same amount of charge (Ah or SOC %) will vary.

The energy and power margin of each battery technology when the sizing is done can as well be analyzed thanks to this method. Figure 23 shows specifically such an Energy/Power plot for the final NMC sizing (1806 kg) with the Mission (1) power trajectory. As can be seen, the power trajectory fits in the Energy/Power pattern and the sizing constraint is here the minimum SOC (20 %). Such a plot can provide quick insight about how the battery technology "fits" for a given power mission and how it would be possible, in a next step, to adapt the power mission in order to optimize the battery utilization for a given sizing.

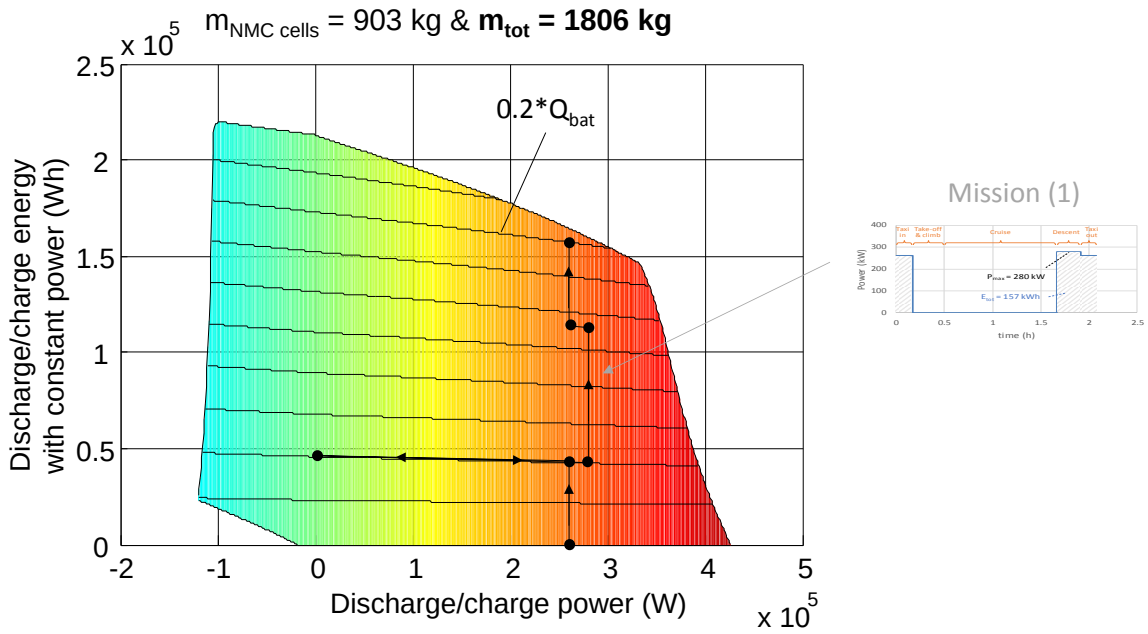

Figure 23 - Energy/Power plot for constant charge/discharge power (final sizing) with mission (1) trajectory

As the battery losses during the mission are here considered, as well as SOC margin for the NMC and BSS cases (LTO and TNO batteries can be fully discharged), the masses estimated Figure 21 are substantially higher than those presented Figure 18. To sum up the global approach, Figure 24 proposes finally a graphical illustration in four steps of the battery modelling and sizing strategy previously described.

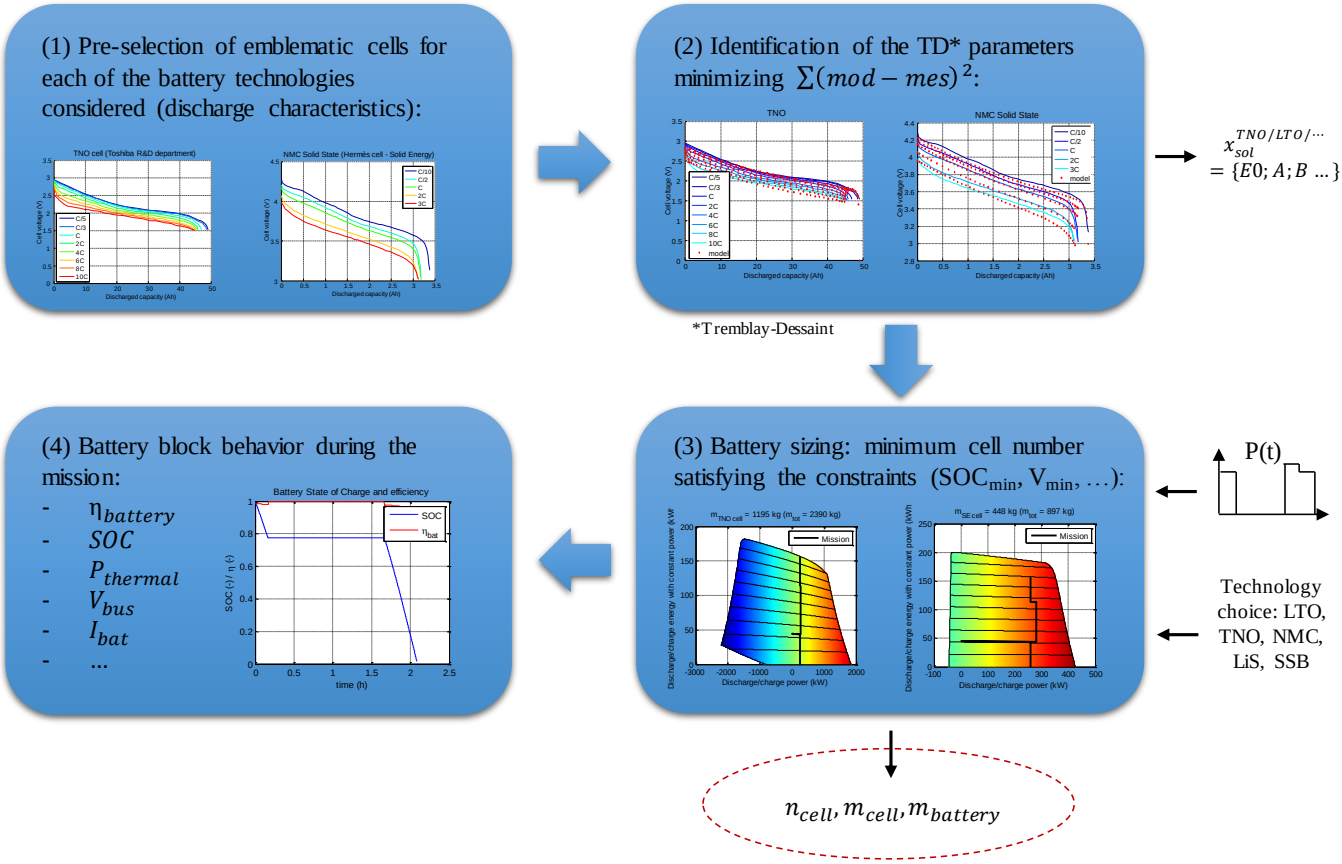

Figure 24 – Recapitulative sketch of the battery modeling and sizing strategies

3.3.2. Fuel Cell system modeling and potential trade-offs

As the state of the art highlights an advanced maturity for LT PEMFC systems as well as the best performances in terms of gravimetric and volumetric power densities, the modeling approach is focused on LT PEMFC systems. In the same vein, a LH_2 storage is considered here as the bibliographic review shows for these H_2 storages the best gravimetric efficiencies. For the FC block, a simplified structure is assumed with one/several FC stack(s), air compressor(s) for the air delivery, H_2 recirculator(s) and a cooling system. A cylindrical LH_2 tank is considered for the H_2 storage as first approximation. Numerous communications are today available on the Toyota Mirai FC car and especially on the FC stack and system. As the Toyota Mirai FC arrangement is today one of the most technologically advanced LT PEMFC embedded system ([YOS-15]), the modeling developments rely largely on information based on this system.

A simplified model of the FC stack mass and volume, depending on the cell number and on the stack surface area, is developed thanks to publications providing insights into the Toyota Mirai stack constitution ([JAM-12], [KOM-15], [BOR-18]). For the performance modeling of the FC stack, a quasi-static equation is employed and its parameters are identified thanks to a communication on the Mirai FC stack performances ([LOH-17]). Knowing the stack voltage, current and efficiency, the FC stack air input mass flow and the H_2 input mass flow can be deduced and used to evaluate the air compressor and the H_2 pump parasitic power consumptions, thanks to respectively a thermodynamic formula (assuming a constant compressor efficiency of 0.55) and an empirical law based on data from [LOH-17]. The FC stack and system efficiencies η_{FC}^{stack} and η_{FC}^{system} are at this step compared with experimental data ([LOH-17]) to validate the whole modeling framework in Figure 25 (the model – in blue – is projected further for higher power values):

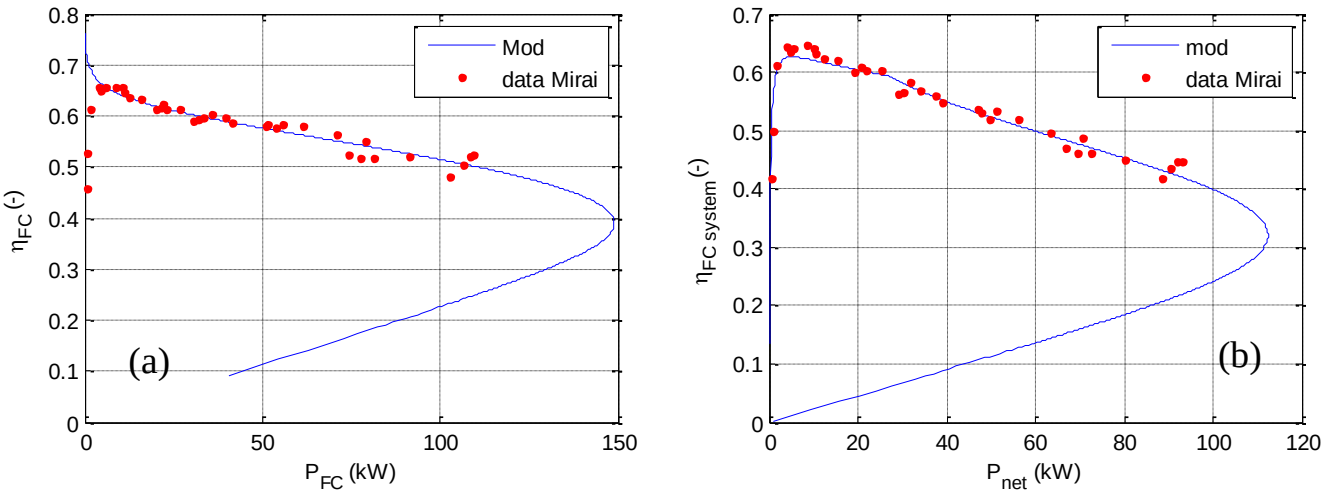

Figure 25 - η_{FC}^{stack} vs P_{FC} (a) and η_{FC}^{system} vs P_{net} (b) characteristics of the Mirai FC stack and system – Model (blue curves) vs experimental data (red points)

The cooling system mass is deduced from the FC stack efficiency (the heat release can be calculated) and an empirical coefficient of ~1.3 $kW_{thermal}/kg$ (identified from Appendix D). For the LH_2 tank mass and volume model, a simplifying hypothesis is made assuming one

cylindrical geometrical design with a constant length to radius ratio (~2.35). Based on [MIC-06], a wall equivalent surface density is assessed, and a tank mass can be calculated knowing the H_2 density inside the tank (a bit lower than the theoretical 71 kg/m^3, as a fraction of the stored H_2 is on gaseous state) and the embedded H_2 mass. Thanks to these modeling developments, a more accurate estimation of the FC system and H_2 storage masses can be made, and interesting couplings can appear inside the FC system between the FC stack size and other parameters, such as the auxiliary parasitic power consumption (hence the system global efficiency), the cooling system mass, the H_2 stored mass for instance. Indeed, when increasing the FC stack size, its efficiency increases, and spillovers effects can be visible on other parts of the system: as lower air and H_2 input flows are necessary, the parasitic consumption of the air compressor and the H_2 recirculation pump decrease and the FC system efficiency increase. Also, the cooling mass decreases as well as the H_2 storage mass when the FC stack efficiency increases. These coupling effects are highlighted in Figure 26, where for a same mission power profile (Mission (1)), several configurations are tested while varying the total number of cells (stack(s) size and number).

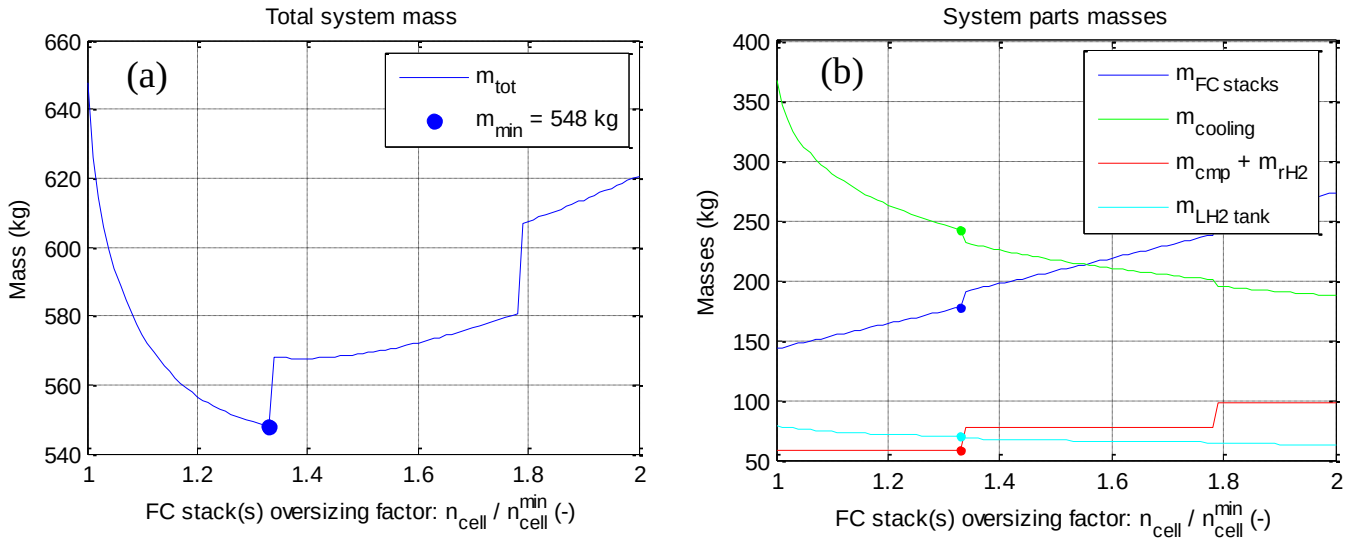

Figure 26 - Evolution of the FC total system mass (a) and of individual parts (b) with the FC stack size for Mission (1)

In this example, a limit is set on the maximal cell number allowed per stack (400 cells in these simulations). For this reason, discontinuities appear when looking to the evolution of the global system mass (and also the individual FC system parts) when one additional stack is added (mainly because of the ending plates weight impact). Interestingly, the system mass shows a non-monotonous variation with the stack oversizing factor (Figure 26 (a)), and reveal the existence of an optimum FC stack design point minimizing the overall system mass.

4. CONCLUSION – PERSPECTIVES

A state of the art of the current performances and future prospects of potential auxiliary sources for the hybrid propulsion has been done. A selection of Li-ion battery technologies, from high power type to very high energy type, as well as a selection of FC technologies has been considered and numerous publications have been scanned in order to assess typical performances values in terms of specific energies and powers. H_2 storages media have as well been investigated regarding their gravimetric efficiencies performances. The bibliographic review showed that reaching maximal values such as 650 Wh/kg_{cell} and 325 Wh/kg_{system} (LiS and/or SSB technologies) may be possible for 2035, but in return, aspects such as C_{rate} capabilities and cyclability will be difficult to improve and may constitute showstoppers for these applications. Although HT PEMFC and SOFC constitute very promising technologies for aviation applications (due to their high working temperature), their current level of maturity and progression margin remains cloudy for the next decades. On the contrary, LT PEMFC is today reaching a certain maturity thanks to the automotive industry and may reach at the system scale values up to 1 kW/kg_{system} in the next decades. On the H_2 storage side, Liquid H_2 storage tanks show the best gravimetric efficiencies and have already been deeply considered in numerous studies for potential aviation applications. Values up to 20 % wt. may be reachable (for H_2 quantities around 10 kg) in the next decades and could highly increase if the H_2 stored quantities increase as well ([VER-10] mention values up to 78 % wt. for H_2 quantities ~1000 kg).

Some masses evaluations have been done considering "light hybridization" scenarios for {FC + H_2 storage} and battery systems, showing the best results for an association between a LT PEMFC and a LH_2 storage. Other modeling developments and more refined masses estimations (visible on Figure 27), on the battery and on the FC sides, show higher values but the same tendencies: the lightest options seem to be the LT PEMFC options (especially with an LH_2 association).

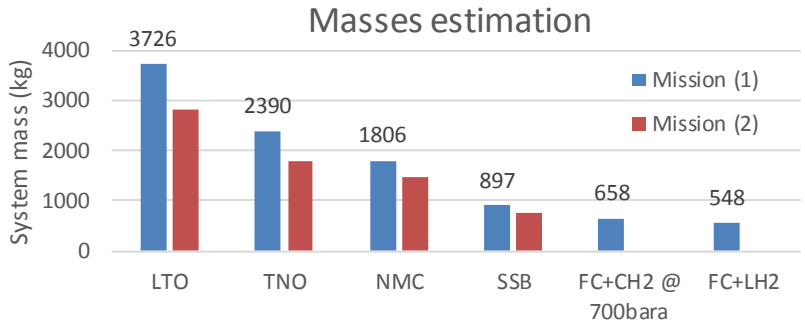

Figure 27 - Battery / FC systems masses estimation for Mission (1) and Mission (2)

Modeling developments have been proposed on the battery and FC sides and have highlighted interesting results regarding potential design trade-offs and sizing procedures.

5. APPENDIX

5.1. Appendix A

Hermes™

High Energy Rechargeable Metal Cells for Space

LMP063767

SolidEnergy Systems developed advanced high-energy lithium-metal rechargeable battery technology, which delivers best-in-class energy density characteristics and cycling performance. This product is ideally suited for applications requiring very high gravimetric and volumetric energy densities that have battery-weight and dimension constraints, such as aeronautics and space, consumer electronics, and EVs.

Benefits

- World's lightest rechargeable battery
- Ultra-high volumetric energy Density of 1200 Wh/L
- Ultra-high gravimetric energy density of 450 Wh/kg
- High Voltage
- Flexible, customizable design
- Recommended for weight constraint applications

Key Features

- Excellent capacity retention and long cycle life
- High pulse charge rate
- High continuous discharge rate
- Great high-altitude performance
- Practical operating temperature range
- High cycling efficiency

Main Applications

- High-altitude drones
- Commercial drones
- Electric autonomous flying transportation
- Consumer electronics
- Power tools
- Small UPS
- Transportation

Electrical Characteristics

Nominal Voltage	3.8 V
Typical Capacity (C10, 25ºC)	3.4 Ah
Nominal Energy	13 Wh

Mechanical Characteristics

Height	66 ± 1 mm
Width	37 ± 1 mm
Thickness	6.35± 0.3 mm
Typical Weight	29 g
Cell Volume	0.015 L

Operating Conditions

Charge Method	Constant Current / Constant Voltage
Charge Voltage	4.3 ± 0.05V
Maximum Recommended Charge Current	0.68 A (0.2 C Rate)
Charge Temperature Range	0ºC to 45ºC
Charge Time at 20ºC	Function of the Charge Current C Rate → 1.5 – 2 Hr C/2 Rate → 2.5 – 3 Hr C/5 Rate → 6 – 7 Hr
Maximum Continuous Discharge Rate	6.8 A (2C Rate)
1kHz ACR, Ω (50%SOS, RT)	<18 mΩ
Pulse Discharge Rate	Up to 16 A (5C Rate)
Discharge Cut-off Voltage	3 V
Discharge Temperature Range	-20ºC to 45ºC

*Electric protection circuits within battery packs may limit the maximum charge/discharge current available. Contact SES.

Hermes™

High Energy Rechargeable Metal Cells for Space

Performance Characteristics

Cycle Life Characteristics

Charge: CC-CV 0.1C (std.) 4.3V, C/20A cut-off at 25°C Discharge: CC 0.5C, 3V cut-off at 25°C

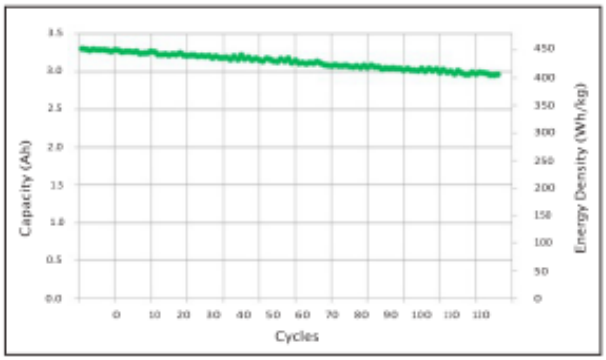

Discharge Rate Characteristics

Charge: CC-CV 0.1C(std.) 4.3V, C/20A cut-off at 25°C
Discharge: CC 0.1C/ 0.5C /1C/ 2C/ 3C, 3V cut-off at 25°C

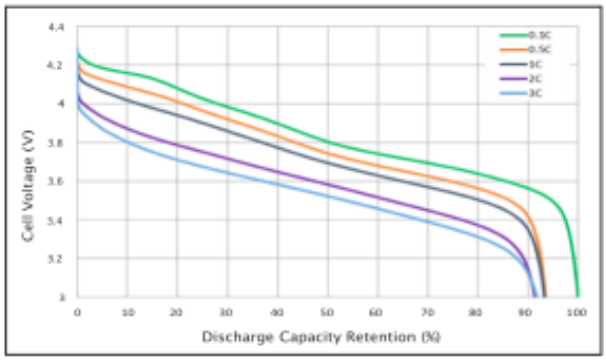

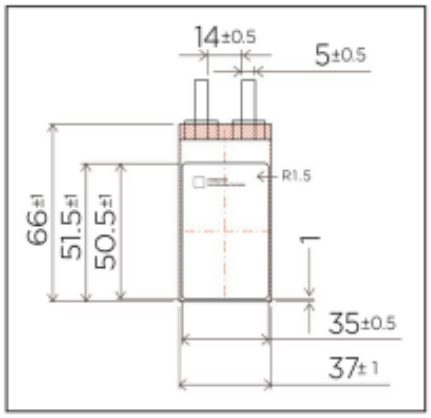

Use dimensions for reference only. For your cell/battery needs please contact SolidEnergy's application engineers.

Discharge Characteristics at 25°C	0.1 C	0.5 C	1.0 C	2.0 C	3.0 C
Capacity, Ah	3.4	3.2	3.2	3.1	3.1
Capacity Retention, %	100	93	93	91	92
Energy, Wh	13.0	12.0	11.8	11.2	11.0
Gravimetric Energy Density, Wh/kg	450	415	408	386	381
Volumetric Energy Density, Wh/L	1157	1068	1050	996	979

Technology

- Ultra-thin lithium metal anode
- Proprietary ultra-light anode current collector
- High Ni content NMC cathode
- Ceramic-filled separator
- Solvent-in-salt electrolyte
- Flexible, customizable design

Storage and Handling

- Store in a dry place at room temperature (preferably <30°C)
- Do not disassemble or incinerate
- Do not short terminals
- For long-term storage, keep the cell within a 30% state of charge

SolidEnergy Systems Corporation

Product Development & Marketing
35 Cabot Road
Woburn, MA 01801 - USA
Tel. +1 339-298-8304
Web: www.solidenergysystems.com

5.2. Appendix B

OXIS ENERGY
Next Generation Battery Technology

Ultra Light Lithium Sulfur Pouch Cell

Ultra Light

High gravimetric energy density, Rechargeable Li-S Pouch Cell

Key Features

- Extremely lightweight: >**400 Wh/kg** already proven
- Safe
- Full 100% Discharge Capability
- High Power type for Aviation and Automotive
- High Energy type for HAPS
- Bespoke cell sizes available

Ultra Light Cell Technology Specifications

Type	High Power	High Energy
Part Number	POA0343	POA0412
Availability	Evaluation Sample	
Operating Voltage (V)	1.9-2.6	
Nominal Voltage (V)	2.1	
Typical Capacity (Ah) 0.2C discharge at 20°C to 1.9V	19.5	14.7
Gravimetric Energy (Wh/kg)	300*	400**
Max. Peak Discharge (C) <30s, 50% SoC, 20°C	6	3
Max. Continuous Discharge (C)***	2	1
Max. Charge Rate (Hours)	4	
Cycle Life (Cycles) 100% DoD****, 80% BoL	80-100	60-100
Cycle Life (Cycles) 80% DoD, 60% BoL	~200	
Operating Temperature (°C)*****	0 to 30	
Storage Temperature (°C)	-30 to 30	
Pouch Format (mm) Length x width x thickness	151x118x10.5	145x78x10
Tab Dimensions (mm) Length x width x heigth	27x20x0.1	
Cell Weight (g)	137	85
Abuse Safety Testing	In-House to IEC62133 standard	

Notes:
* Figure obtained at 0.2C discharge at 30°C
** Figure obtained at 0.1C discharge at 20°C
*** Maximum discharge rates are expressed as a C-Rate, defined as a ratio of the maximum discharge power (W) to the typical cell capacity (Wh).
**** Depth of Discharge (DoD) is the percentage of the cell's rated capacity discharges relative to a fully charged condition.
***** The same range applies for both charge and discharge.

PRODUCT DATA SHEET
Rechargeable Lithium Sulfur Rack Mounted Battery

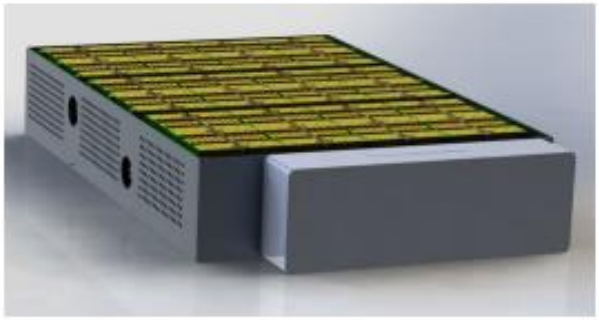

- **State-of-the-art Lithium Sulfur technology**
- **19" rack-mount battery with only a 3U profile**
- **Nominal 48V / 3 kWh Lithium Sulfur pack**
- **For Energy Storage and Vehicle applications**
- **Fully scalable to large MWh solutions**
- **Lightweight – only 25 kg**
- **Extremely safe - no acids or risk of fire**
- **Reduced environmental impact**
- **Advanced Battery Management System providing safe operation, control and status**

Description:

The unit is based on OXIS Energy's unique Lithium Sulfur (Li-S) technology, offering a superior gravimetric energy density resulting in a very lightweight battery. Furthermore, compared to other lithium based chemistries, OXIS cells are very robust and safe when subject to abuse such as over-discharge, over-charge and high temperatures.

The active ingredients of the Li-S cells are sulfur - a recycled waste product from the oil industry - and lithium. Unlike lithium-ion our cells do not contain manganese, cobalt, lead or other harmful metals.

The battery is designed to easily install into 19" racking, allowing a scalable solution to both cabinet and large container size systems.

Communication ports are included, providing full diagnostics, status indication, health and usage monitoring. The on-board communication allow users access to various battery information including cell fault report, data logging, voltage, battery State of Charge (SoC) and historical data.

The advanced Battery Management System provides the measurement and safe control of cells, ensuring that they are closely matched and balanced during charging.

Parameter	Performance
Nominal Voltage	48 V
Rated Capacity	3000 Wh
Weight	25 kg
Max. Continuous Discharge	3000 W
Max Peak (30 sec) Discharge	9000 W
Dimensions	H = 130 mm W = 482 mm D= 650 mm
Charge Time	4 Hours
Cycle life (80% DoD, 60% BoL)	1,400
Operating Temperature range	0 to +60 °C
Communication Interface	CANbus, RS485, Ethernet
Approval	CE Designed to meet UN DoT38.3
Safety and Protection	The unit incorporates electronic protection, including: • Over-charge protection • Over-discharge protection • External short circuit protection • Over temperature monitoring

OXIS ENERGY
Next Generation Battery Technology

5.3. Appendix C

Lithium Sulfur Rechargeable Battery Data Sheet

Lithium sulfur has the highest theoretical specific and volumetric energy densities of any rechargeable battery chemistry (2550 Wh/kg and 2862 Wh/l theoretically). SION Power has learned how to unlock this potential and has created a unique rechargeable battery system. This patented technology is enabling new applications for rechargeable batteries and replacing existing primary and rechargeable batteries in applications where weight is a critical factor.

Typical applications include:

- Unmanned Vehicle Systems
- Weight sensitive electronic applications
- Military communication systems
- Sensors

Electrical Specifications:

Nominal Voltage:	2.15V
Maximum Charge Voltage:	2.5V
Minimum Voltage on Discharge:	1.7V
Nominal Capacity @ 25°C:	2.5 Ah @ C/5
Maximum continuous discharge rate:	2C
Maximum charge rate:	C/5
Specific Energy:	350 Wh/kg
Energy Density:	320 Wh/l
Cell Impedance:	25 mΩ

Mechanical Specifications:

Configuration:	Prismatic
Length:	55 mm (top flanged folded)
Width:	37 mm
Thickness:	11.5 mm
Weight:	~16 g

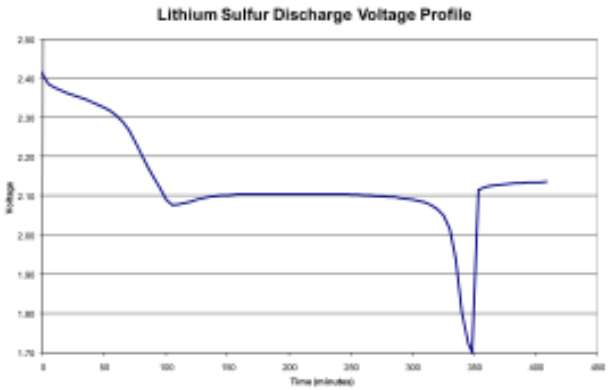

Environmental Specifications:

Discharge Temperature:	-20°C to +45°C
Charge Temperature:	-20°C to +45°C
Storage Temperature:	-40°C to +50°C

SION Power Inc., 2900E. Elvira Rd., Tucson, AZ 85756 Tel: +1.520.799.7500 Fax: 1.520.799.7501
www.sionpower.com

Date: 10/3/08 - Supersedes: 09/28/05

5.4. Appendix D

Intelligent Energy

Data sheet

100kW EC Automotive Fuel Cell System

The Intelligent Energy 100kW fuel cell architecture has been developed in response to increasing market demand for next generation high power automotive fuel cell solutions.

The 100kW platform takes full advantage of Intelligent Energy's superior stack technology which offers world leadership in power density.

A history of 25 years in fuel cell technology development has produced compact and power-dense fuel cells which offer robust and cost-effective power systems for the automotive market.

Features:

- Patented E C fuel cell technology
- No cooling required – simplified balance of plant
- World-class stack power density
- Designed for ease of integration into automotive applications

Includes:

- Fuel cell stack featuring Intelligent Energy's proprietary EC technology
- Hydrogen regulation
- Air management system including compressor and controller
- Water management and recovery system
- Stack thermal management system
- Low voltage control module
- HV interface

100kW Fuel Cell Power Unit

Description	A hydrogen fuelled PEM fuel cell power unit, designed to automotive standards for both mobile and stationary applications, for example as an automotive FCEV power plant, or stationary DC generator.	
System architecture	Fuel cell system	Including fuel cell stack, fuel management, air management, water management, thermal management and control module
	Fuel cell stack	Intelligent Energy proprietary evaporatively-cooled fuel cell stack – demonstrated at 3.0kW/kg and 3.5kW/L
Electrical output	Rated continuous net power output	100kWe
	Maximum voltage	320 VDC
	Minimum voltage	180 VDC
Physical system	Mass	150kg [1]
	Maximum dimensions	400 (W) × 700 (D) × 600 (H) mm
Environment	Operating ambient temperature range	-20°C to 30°C nominal -40°C to 85°C derated
	Storage / shipment	-40°C to 85°C
Fuel	Type	Gaseous hydrogen ISO14687:2 Grade D
	Efficiency at rated power [2]	40% [2]
	Peak efficiency	55% [2]
	Fuel flow rate at rated power	7.5kg/h
	Hydrogen supply pressure	6 to 10BarG
Interfaces	Electrical	1 off high voltage power output with integral interlock 1 off low voltage interface (11 to 14V DC) bi-directional earthing point for chassis ground
	Control	CAN 2.0B bus

[1] Complete system mass including condenser.

[2] Efficiency of system at 25°C, 100kPa, including balance of plant and condenser.

6. BIBLIOGRAPHY

[AMA-06] Amaseder, F., & Krainz, G. (2006). Liquid hydrogen storage systems developed and manufactured for the first time for customer cars (No. 2006-01-0432). SAE Technical Paper.

[BAL-16] Ballard FCveloCity® specifications (2016). (http://www.ballard.com/docs/default-source/motive-modules-documents/fcvelocity_hd_family_of_products_low_res.pdf)

[BEN-15] Bensadoun, E. (2015). Hydrogen Storage on board aeronef and ground infrastructure. *Air Liquide Advanced Technologies - Workshop on aeronautical applications of fuel cell and hydrogen technologies*. Lampholdshausen, Germany.

[BIR-10] Birke, P. (Continental). Electric Battery Actual and future Battery Technology Trends (2010).

[BOR-18] Borup, Rodney L., et al. PEM Fuel Cell Catalyst Layer (MEA) Architectures. No. LA-UR-18-24447. Los Alamos National Lab.(LANL), Los Alamos, NM (United States), 2018.

[BOW-06] Bowman Jr, R. C. (2006, May). Roles of hydrogen in space explorations. In AIP Conference Proceedings (Vol. 837, No. 1, pp. 175-199). AIP.

[BOW-12] Bowman, B., & Klebanoff, L. (2012). Historical Perspectives on Hydrogen, Its Storage, and Its Applications. Hydrogen Storage Technology: Materials and Applications, 65.

[BUS-16] BusinessWire New. Solid hydrogen-on-demand fuel cell from HES energy systems flies ST Aerospace UAV for record 6 hours. February 2016. http://www.businesswire.com/news/home/20160216006857/en/Solid-Hydrogen-on-Demand-Fuel-Cell-HES-Energy-Systems

[DIC-18] Dicks, A., & Rand, D. A. J. (2018). Fuel cell systems explained. Chapter 11: Hydrogen Storage. New York: Wiley.

[DOE-16] Department of Energy (2017). Fuel Cell Technologies Office Multi-Year Research, Development, and Demonstration Plan. https://www.energy.gov/sites/prod/files/2017/05/f34/fcto_myrdd_fuel_cells.pdf

[EEL-04] Eelman, S., y de Poza, I. D. P., & Krieg, T. (2004). fuel cell APU'S in commercial aircraft an assessment of SOFC and PEMFC concepts. In 24th international congress of the Aeronautical sciences, ICAS 2004.

[ESA-18] ESA Roadmap of activities (2018). CNES, COMET, Batteries, constraints, challenges and perspectives, Toulouse.

[FON-13] Da Fonseca, R. (2013). Optimization of the sizing and energy management strategy for a hybrid fuel cell vehicle including fuel cell dynamics and durability constraints. *These de doctorat de l'Institut National des Sciences Appliquées de Lyon*.

[FOT-17] Fotouhi, A., Auger, D., O'Neill, L., Cleaver, T., & Walus, S. (2017). Lithium-sulfur battery technology readiness and applications—a review. *Energies*, *10*(12), 1937.

[FRA-18] Fraunhaufer institute / Thales Arena (2018). Management of a Li-S battery for space applications. CNES, COMET, *Batteries, constraints, challenges and perspectives*, Toulouse.

[FUS-15] Fusalba, F. (2015). Key Drivers for Aerospace Batteries: Today and Future Aircraft Electrically Powered. In *Proceedings of the EU-Japan Symposium "Electrical Technologies for the Aviation of the Future*.

[HAG-06] Haglind, F., Hasselrot, A., & Singh, R. (2006). Potential of reducing the environmental impact of aviation by using hydrogen Part I: Background, prospects and challenges. The Aeronautical Journal, 110(1110), 533-540.

[HAS-15] Hasegawa, T., Nissan research center, (2015). Airbus symposium: future perspectives on fuel cell technologies. *Europe-Japan Symposium Electrical Technologies for the Aviation of the Future*, Tokyo, March 2015.

[HAS-16] Hasegawa, T., Imanishi, H., Nada, M., and Ikogi, Y., "Development of the Fuel Cell System in the Mirai FCV," SAE Technical Paper 2016-01-1185, 2016, doi:10.4271/2016-01-1185.

[HEP-12] Hepperle, M. (2012). Electric flight-potential and limitations.

[HEX-17] Hydrogen storage and transportation systems. Hexagon Composite brochure (2017). (http://www.hexagonlincoln.com/resources/brochures)

[HOE-18] Hoelzen, J., Liu, Y., Bensmann, B., Winnefeld, C., Elham, A., Friedrichs, J., & Hanke-Rauschenbach, R. (2018). Conceptual design of operation strategies for hybrid electric aircraft. *Energies*, *11*(1), 217.

[Hy4] Hy4 Fuel Cell aircraft website. (http://hy4.org/hy4-technology)

[HYD-16] Hydrogenics (2016). HyPM-HD POWER MODULES for light and heavy duty mobility, technical specifications. (https://www.hydrogenics.com/wp-content/uploads/HyPM-HD-Brochure.pdf)

[IE-15] Intelligent Energy 100 kW EC Automotive Fuel Cell System datasheet (2015).

[IE-18] Intelligent Energy official website, Evaporatively Cooled technology page. https://www.intelligent-energy.com/evaporatively-cooled-technology/

[JAM-12] James, Brian D., and Andrew B. Spisak. "Mass production cost estimation of direct H2 PEM fuel cell systems for transportation applications: 2012 update." report by Strategic Analysis, Inc., under Award Number DEEE0005236 for the US Department of Energy 18 (2012).

[KAD-18] Kadyk, T., Winnefeld, C., Hanke-Rauschenbach, R., & Krewer, U. (2018). Analysis and Design of Fuel Cell Systems for Aviation. *Energies*, *11*(2), 375.

[KHA-13] Khandelwal, B., Karakurt, A., Sekaran, P. R., Sethi, V., & Singh, R. (2013). Hydrogen powered aircraft: the future of air transport. *Progress in Aerospace Sciences*, *60*, 45-59.

[KOJ-15] Kojima, K., & Fukazawa, K. (2015). Current status and future outlook of fuel cell vehicle development in TOYOTA. *ECS Transactions*, *69*(17), 213-219.

[KOK-15] KOKAM Li-ion / Polymer cell brochure (http://kokam.com/cell/)

[KOK-17] Kokam battery solution - Transportation application / Kokam modular pack - For High Energy E-mobility (http://kokam.com/data/Kokam_EV_Pack_Brochure_V_1.6.pdf)

[KON-15] Konno, Norishige, Seiji Mizuno, and Hiroya Nakaji. "Development of compact and high-performance fuel cell stack." SAE International Journal of Alternative Powertrains 4.1 (2015): 123-129.

[KUH-12] Kuhn, H., & Sizmann, A. (2012). *Fundamental prerequisites for electric flying*. Deutsche Gesellschaft für Luft-und Raumfahrt-Lilienthal-Oberth eV.

[LEC-14(2)] http://www.leclanche.com/technology-products/products/graphitenmc-racks/

[LEC-14] http://www.leclanche.com/technology-products/leclanche-technology/lithium-ion-cells/

[LEC-15] Le Cras, F., Bloch, D. (2015). De Volta aux accumulateurs Li-ion - Développement des batteries au Lithium. *Techniques de l'ingénieur, Réf: BE8620.*

[LOH-17] Lohse-Busch, H., Stutenberg, K., Duoba, M., & Iliev, S. (2018). *Technology Assessment Of A Fuel Cell Vehicle: 2017 Toyota Mirai* (No. ANL/ESD-18/12). Argonne National Lab.(ANL), Argonne, IL (United States).

[MAK-17] Makridis, S. (2017). Hydrogen storage and compression. arXiv preprint arXiv:1702.06015.

[MAT-09] Matsunaga, M., Fukushima, T., & Ojima, K. (2009). Powertrain system of Honda FCX Clarity fuel cell vehicle. *World Electric Vehicle Journal*, *3*(4), 820-829.

[MIC-06] Michel, F., Fieseler, H., & Allidieres, L. (2006, June). Liquid hydrogen technologies for mobile use. In Proceedings of WHEC (Vol. 16, pp. 13-16).

[MIC-08] Michel, F. (2008). Cryogenic Reservoirs. In Hydrogen Technology (pp. 311-333). Springer, Berlin, Heidelberg.

[MIS-18] Misra, A. (2018). Energy Storage for Electrified Aircraft: The Need for Better Batteries, Fuel Cells, and Supercapacitors. *IEEE Electrification Magazine*, *6*(3), 54-61.

[MUE-18] Mueller, J. K., Bensmann, A., Bensmann, B., Fischer, T., Kadyk, T., Narjes, G., ... & Hanke-Rauschenbach, R. (2018). Design considerations for the electrical power supply of future civil aircraft with active high-lift systems. *Energies*, *11*(1), 179.

[MUL-07] Müller, C., Fürst, S., & von Klitzing, W. (2007). Hydrogen Safety: New challenges based on BMW Hydrogen 7. In Proceedings.

[NEO-17] Neophytides, S., Daletou, M. K., Athanasopoulos, N., Gourdoupi, N., De Castro, E., & Schautz, M. (2017). High Temperature PEM Fuel Cell Stacks with Advent TPS Meas. In E3S Web of Conferences (Vol. 16, p. 10002). EDP Sciences.

[NOJ-09] Nojoumi, H., Dincer, I., & Naterer, G. F. (2009). Greenhouse gas emissions assessment of hydrogen and kerosene-fueled aircraft propulsion. *International journal of hydrogen energy*, *34*(3), 1363-1369.

[NON-17] Nonobe, Y. (2017). Development of the fuel cell vehicle mirai. *IEEJ Transactions on Electrical and Electronic Engineering*, *12*(1), 5-9.

[OXI-17] Datasheet Ultra-light Lithium Sulfur pouch cell Oxis Energy (available on: https://oxisenergy.com/products/)

[PAN-18] Panasonic UR18650ZTA cylindrical cell datasheet (https://industrial.panasonic.com/ww/products/batteries/secondary-batteries/lithium-ion/cylindrical-type/UR18650ZTA)

[PER-18] Perdu, F. (2018). OVERVIEW OF EXISTING AND INNOVATIVE BATTERIES, CEA Liten, *Science and energy scenarios.*

[POG-18] Poggel, S., Aptsiauri, G., Flade, S., Schirmer, S. (2018). Electric powertrain technology for fixed-wing aircraft. *International Hydrogen and Fuel Cell Conference*, Trondheim.

[POR-15] Pornet, C., & Isikveren, A. T. (2015). Conceptual design of hybrid-electric transport aircraft. *Progress in Aerospace Sciences*, *79*, 114-135.

[POW-16(1)] PowerCell S3 stack (2016) datasheet. (https://www.powercell.se/wordpress/wp-content/uploads/2018/12/powercell-s3-datasheet-pdf-190129.pdf)

[POW-16(2)] PowerCell MS 100 FC System (2016). (https://www.powercell.se/wordpress/wp-content/uploads/2018/12/powercell-ms100-datasheet-pdf.pdf)

[RAJ-08] Rajashekara, K., Grieve, J., & Daggett, D. (2008). Hybrid fuel cell power in aircraft. IEEE Industry Applications Magazine, 14(4), 54-60.

[REN-16] Renau, J., Barroso, J., Lozano, A., Nueno, A., Sánchez, F., Martín, J., & Barreras, F. (2016). Design and manufacture of a high-temperature PEMFC and its cooling system to power a lightweight UAV for a high altitude mission. International Journal of Hydrogen Energy, 41(43), 19702-19712.

[ROS-17] Rosli, R. E., Sulong, A. B., Daud, W. R. W., Zulkifley, M. A., Husaini, T., Rosli, M. I., ... & Haque, M. A. (2017). A review of high-temperature proton exchange membrane fuel cell (HT-PEMFC) system. International Journal of Hydrogen Energy, 42(14), 9293-9314.

[ROT-10] Roth, B., & Giffin, R. (2010, July). Fuel cell hybrid propulsion challenges and opportunities for commercial aviation. In 46th AIAA/ASME/SAE/ASEE Joint Propulsion Conference & Exhibit (p. 6537).

[SAD-17] Sadaghiani, M. S., & Mehrpooya, M. (2017). Introducing and energy analysis of a novel cryogenic hydrogen liquefaction process configuration. International Journal of Hydrogen Energy, 42(9), 6033-6050.

[SE-18(2)] Solid Energy - Li-metal/NMC cell datasheet (Hermès) / (http://www.solidenergysystems.com/hermes/)

[SE-18] Solid Energy - how solid Energy is transforming the future of transportation and connectivity (http://www.solidenergysystems.com/athena/)

[SHA-15] Sharifzadeh, S., Verstraete, D., & Hendrick, P. (2015). Cryogenic hydrogen fuel tanks for large hypersonic cruise vehicles. International Journal of Hydrogen Energy, 40(37), 12798-12810.

[SIN-17] Sinigaglia, T., Lewiski, F., Martins, M. E. S., & Siluk, J. C. M. (2017). Production, storage, fuel stations of hydrogen and its utilization in automotive applications-a review. International journal of hydrogen energy, 42(39), 24597-24611.

[SIO-08] Datasheet SionPower prismatic Lithium Sulfur cell

[SIO-18] https://sionpower.com/products/

[STR-14] Stroman, R. O., Schuette, M. W., Swider-Lyons, K., Rodgers, J. A., & Edwards, D. J. (2014). Liquid hydrogen fuel system design and demonstration in a small long endurance air vehicle. international journal of hydrogen energy, 39(21), 11279-11290.

[STU-12] Stückl, S., van Toor, J., & Lobentanzer, H. (2012, September). VOLTAIR–the all electric propulsion concept platform–a vision for atmospheric friendly flight. In *28th International Congress of the Aeronautical Sciences (ICAS)*.

[TAK-18] Takami, N., Ise, K., Harada, Y., Iwasaki, T., Kishi, T., & Hoshina, K. (2018). High-energy, fast-charging, long-life lithium-ion batteries using TiNb 2 O 7 anodes for automotive applications. *Journal of Power Sources*, *396*, 429-436.

[TAR-16] Tariq, M., Maswood, A. I., Gajanayake, C. J., & Gupta, A. K. (2016). Aircraft batteries: current trend towards more electric aircraft. *IET Electrical Systems in Transportation*, *7*(2), 93-103.

[TOS-17] Toshiba rechargeable battery SCiB™ - datasheet cells and module (https://www.scib.jp/en/product/index.htm)

[TRE-09] Tremblay, O., & Dessaint, L. A. (2009). Experimental validation of a battery dynamic model for EV applications. World electric vehicle journal, 3(2), 289-298.

[VER-10] Verstraete, D., Hendrick, P., Pilidis, P., & Ramsden, K. (2010). Hydrogen fuel tanks for subsonic transport aircraft. International journal of hydrogen energy, 35(20), 11085-11098.

[WES-03] Westenberger, A. (2003). Liquid hydrogen fuelled aircraft-system analysis. *CRYOPLANE, The European Commission, Brussels, Belgium, Report No. GRD1-1999-10014*.

[WIN-18] Winnefeld, C., Kadyk, T., Bensmann, B., Krewer, U., & Hanke-Rauschenbach, R. (2018). Modelling and designing cryogenic hydrogen tanks for future aircraft applications. *Energies*, *11*(1), 105.

[YOS-15] Yoshida, T., & Kojima, K. (2015). Toyota MIRAI fuel cell vehicle and progress toward a future hydrogen society. *The Electrochemical Society Interface*, *24*(2), 45-49.

[YOU-04] Young, R. C., Chao, B., Li, Y., Myasnikov, V., Huang, B., & Ovshinsky, S. R. (2004). A hydrogen ICE vehicle powered by Ovonic metal hydride storage. SAE transactions, 348-358.